

AN INDUCTOR-TYPE ALTERNATOR

by

Frank E. Steinberg

S.B., MASSACHUSETTS INSTITUTE OF TECHNOLOGY

(1951)

SUBMITTED IN PARTIAL FULFILLMENT OF THE

REQUIREMENTS FOR THE DEGREE OF

MASTER OF SCIENCE

at the

MASSACHUSETTS INSTITUTE OF TECHNOLOGY

September, 1953

Signature redacted

Signature of Author.....  
Department of Electrical Engineering, Sept.1953

Certified by.....  
Signature redacted  
Thesis Supervisor

Accepted by.....  
Signature redacted  
Chairman, Department Committee on Graduate Students



Room 14-0551  
77 Massachusetts Avenue  
Cambridge, MA 02139  
Ph: 617.253.5668 Fax: 617.253.1690  
Email: docs@mit.edu  
<http://libraries.mit.edu/docs>

## **DISCLAIMER OF QUALITY**

Due to the condition of the original material, there are unavoidable flaws in this reproduction. We have made every effort possible to provide you with the best copy available. If you are dissatisfied with this product and find it unusable, please contact Document Services as soon as possible.

Thank you.

**Due to the poor quality of the original document, there is some spotting or background shading in this document.**

TABLE OF CONTENTS

ABSTRACT	
INTRODUCTION	1
I DESCRIPTION OF THE ALTERNATOR	3
II CALCULATION OF OPEN-CIRCUIT VOLTAGE	7
III THE ALTERNATOR ON LOAD	25
IV TEST RESULTS AND THEIR COMPARISON WITH THE THEORY	43
V CONCLUSIONS	56
APPENDIX I:	
CALCULATION OF AIR-PATH PERMEANCES	58
OPEN-CIRCUIT LEAKAGE PERMEANCE	60
DRAWINGS	62
APPENDIX II:	
CALCULATION OF ARMATURE REACTION LEAKAGE PERMEANCE	63
APPENDIX III:	
DATA AND EQUIVALENT CIRCUIT CALCULATIONS	64
BIBLIOGRAPHY	

## AN INDUCTOR-TYPE ALTERNATOR

by

Frank E. Steinberg

Submitted to the Department of Electrical Engineering on Sept. 7, 1953 in partial fulfillment of the requirements for the degree of Master of Science.

### ABSTRACT

A steady-state analysis of a permanent-magnetic-excited inductor alternator is presented.

The no-load flux linking the armature winding as a function of rotor position is determined by graphical analysis. Once the relationship between flux and rotor position (or equivalently time) is obtained it may be expressed in form of a Fourier series. The open-circuit voltage wave is known with the no-load flux.

With the alternator loaded the ampere turns resulting from armature reaction are shown to act on a flux path different from the path of the no-load flux. This condition is accounted for by introducing an incremental armature reaction permeance which is found to have an average value and a double-frequency component. Odd harmonic flux components result from current acting on this second order permeance. Possible demagnetization of the magnets due to armature reaction under abnormal conditions is discussed briefly.

A vector diagram for the fundamental components is included. Neglecting the double-frequency component of the armature reaction permeance permits to represent the alternator by a simple equivalent circuit for rms quantities. The performance of the alternator is then calculated from this equivalent circuit and compared with experimental results.

Thesis Supervisor: David C. White.

Title: Assistant Professor of Electrical Engineering.

## ACKNOWLEDGMENT

The Hughes Aircraft Company, Culver City, California, loaned the turbo alternator to the Dynamic Analysis and Control Laboratory at the Massachusetts Institute of Technology for the purpose of this investigation. The author wishes to thank them for their sponsorship. He is also indebted to D. and R., Ltd., Santa Barbara, California, the manufacturer, for supplying drawings and other information about the alternator.

Professor David C. White's supervision and considerate guidance throughout this investigation are greatly appreciated.

Thanks are also due to Mr. Fred L. Schultz for preparing many of the drawings in this thesis.

## INTRODUCTION

At the beginning of this century the need for a high-frequency power source in telecommunication led to studies of high-speed rotary power supplies. It was immediately recognized that the inductor-type alternator is well suited for this purpose. In a machine of this type the rotor consists of a laminated cylinder, slotted at the periphery and is devoid of windings. Consequently, the rotor is of simple and robust construction and may be subjected to high peripheral speeds. Also, since each rotor tooth represents a pole, a large number of poles can be accommodated. Emfs are induced in the armature winding due to a rate of change of flux linkages caused by the periodic pulsations of air-gap permeances within a unidirectional field, set up generally by a d-c excited winding on the stator. Since the frequency of the induced emf is proportional to the product of rotor speed and the number of rotor poles it follows that the inductor alternator is capable of producing high (up to 50 kcps) frequencies.

More recently industrial applications like induction furnaces, surface hardening, dielectric heating, etc. created a growing demand for high-frequency, heavy-current alternators. Consequently, a variety of inductor-type machines was developed. In all these applications the primary object is to obtain a sufficiently high frequency, the physical size of the machine mainly entering as a cost factor.

During recent years a new application of high-frequency power supplies has resulted from the need of maximizing the power output per unit volume. This situation exists where space is at a premium. The inductor alternator to be investigated evolved from requirements resulting from this last application. It was constructed by D. and R. Ltd., according to the following specifications:

Output frequency: 6000 cps, single phase  
Output voltage: between 100 and 200 volts  
for load from 60 to 100 watts  
Overall diameter: 2 inches  
Overall length: 1.6 inches

The manufacturer supplied a set of drawings of an alternator type similar to the one tested in this report. Calculations from design data are based on these drawings.

Other outstanding features of this alternator are:

(1) excitation is provided by means of permanent magnets, (2) the flux linking the armature winding is alternating (changing between a positive and negative maximum value), and not merely pulsating unidirectionally as is the case for most inductor alternators.

## I. DESCRIPTION OF THE ALTERNATOR

### Construction

Figure 1 shows a cross-sectional view of the active parts of the generator. The rotor has six equally spaced poles and is made from a stack of transformer-iron laminations. Surrounding the rotor, separated by a 0.0025" air gap, is the stator consisting of two laminated soft-iron structures embracing two Alnico V bar magnets. The protruding ends of the soft-iron structures form the four stator poles. Each stator yoke carries a winding of 180 turns of No 31 wire whose terminals are connected to binding posts mounted on the outside of the alternator housing. The entire assembly is cased in a cylindrical aluminum housing and all the air space with the exception of the cylindrical air gap is filled with a thermo-setting plastic resin.

### Principle of Operation

For the alternator described e.m. fs are induced in the armature windings due to a rate of change of flux linkages caused by periodic changes of air-gap permeances. Accordingly, this machine falls into the class of inductor-type alternators. Excitation is provided by means of the two permanent magnets, which have been polarized so that the magnetic axis of each is pointing in the upward direction. With the rotor in the position shown in Figure 2a, the center line of a diametrically opposite pair of rotor poles



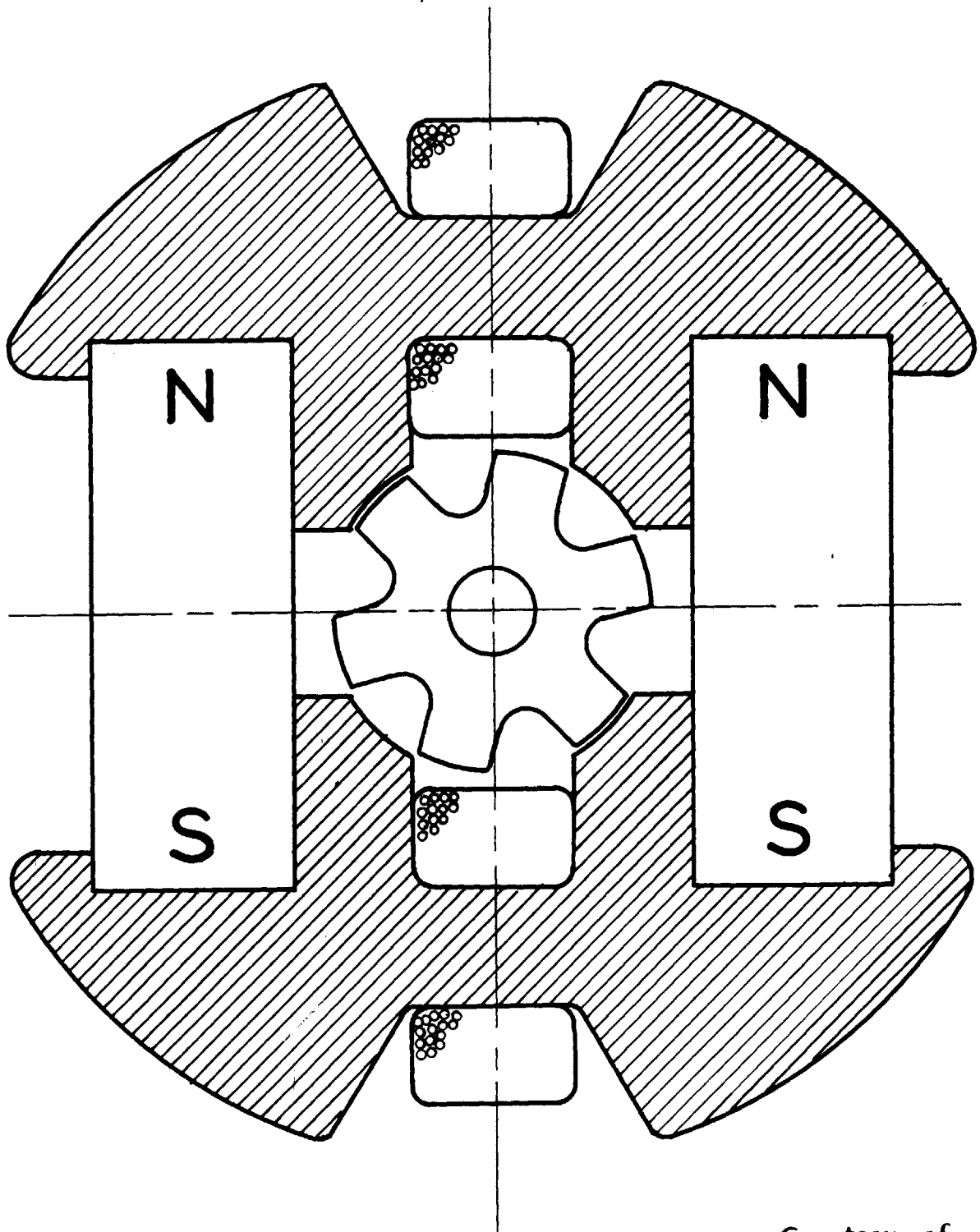


FIGURE 1

Courtesy of  
D & R, LTD.  
Santa Barbara, Calif.

4x SIZE  
AIR GAP 0.0025" not to scale

exactly lines up with the center line of a pair of stator poles. The other pair of stator poles faces the rotor slots. The dashed lines indicate the path of the main flux. Figure 2b and 2c show the path of the main flux for the rotor rotated in the clockwise direction by 15 mechanical degrees and 30 mechanical degrees respectively from the position shown in Figure 2a. These figures show how the flux linking the armature coils varies with the rotor

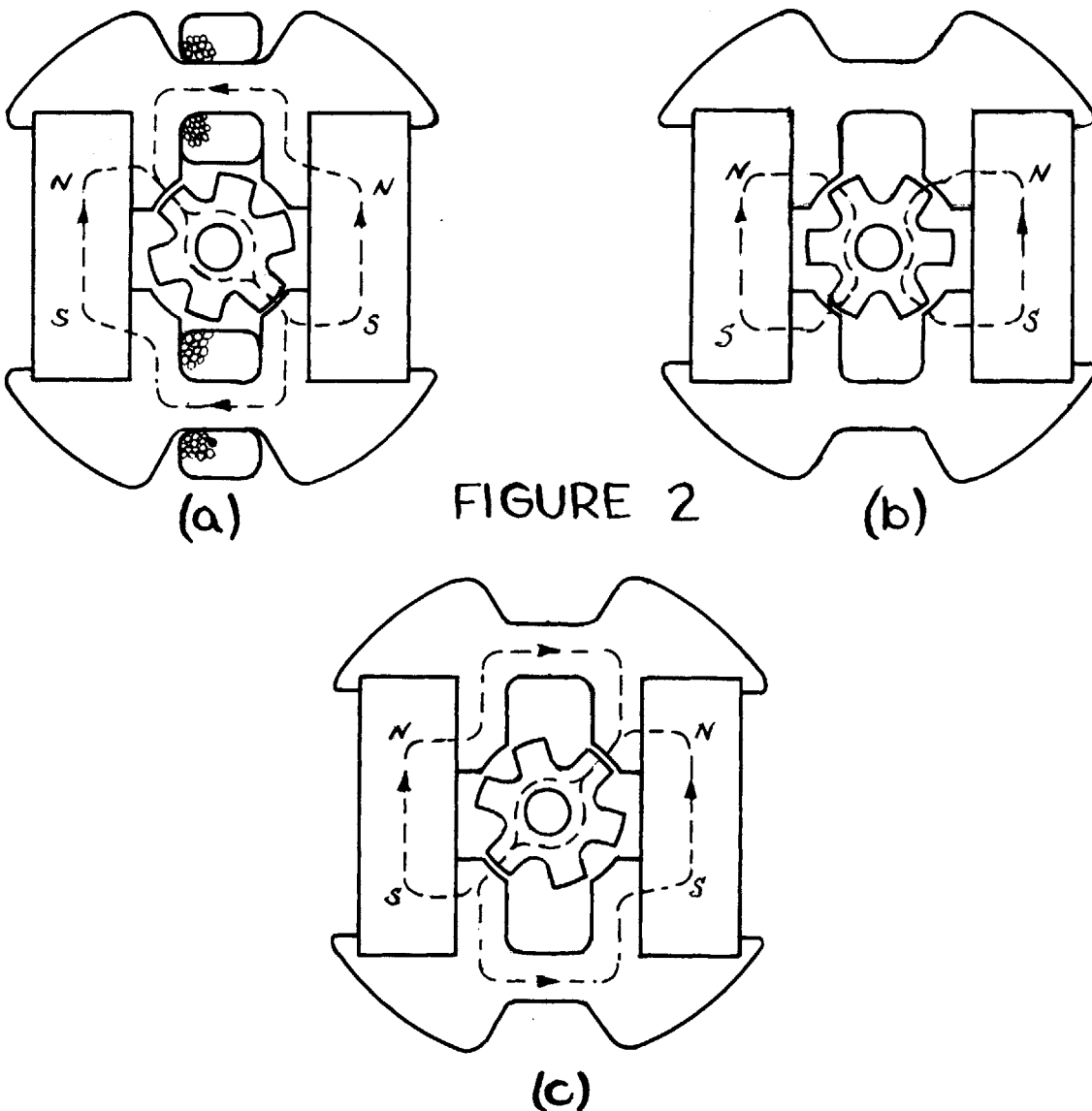


FIGURE 2

position. With the rotor in the position shown in Figure 2a the flux linking each armature coil is directed from right to left and has its maximum value. With the rotor displaced 15 mechanical degrees in the clockwise direction (Fig.2b) the flux linking each armature coil is zero. For the rotor position of Figure 2c the flux has again its maximum value but the direction is now from left to right. A further rotation of the rotor by 30 mechanical degrees in the clockwise direction results in the same flux pattern as shown in Figure 2a. Thus if the rotor is rotated through a tooth-slot combination the flux in each stator yoke goes through one complete cycle. Consequently the frequency of the e.m.f. induced in the armature windings is equal to the speed of the rotor in rps times the number of rotor poles, or

$$f = \frac{p n}{60} \dots \dots \dots (1)$$

f = frequency in cps

p = number of poles

n = rotor speed in rpm.

It should be noted that for this inductor machine the flux linking the armature coils is alternating rather than just pulsating. Also for rotor speed and number of rotor poles given, the output frequency of this machine is twice that of a conventional alternator.

## II. CALCULATION OF OPEN-CIRCUIT VOLTAGE

To demonstrate the method of attack to be followed in the solution of the magnetic circuit problem of the alternator let us first consider a simpler, but closely related problem.

### PROBLEM

In Figure 3 the cylindrical plunger is subjected to a forced displacement  $x = 0.05(1.4 - \cos \omega t)$  cm where  $x$  is the length of the air gap between the stationary cylinder and the moving plunger. Neglecting all leakage and fringing flux, determine the flux in either yoke as a function of time.

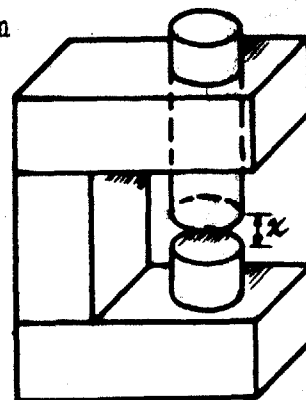


FIGURE 3

### SOLUTION

When the approximate magnetic field configuration throughout the greater portion of the region of interest is simple and can be determined by inspection the concepts, terminology, and symbolism of circuitry may be applied. Under these conditions it is helpful to make use of the analogy existing between the quantities current, voltage, resistance or conductance of the electric circuit and the quantities flux, mmf, reluctance or permeance respectively of the magnetic circuit. Thus the arrangement of Figure 3 can be represented by the equivalent circuits shown in Figure 4.

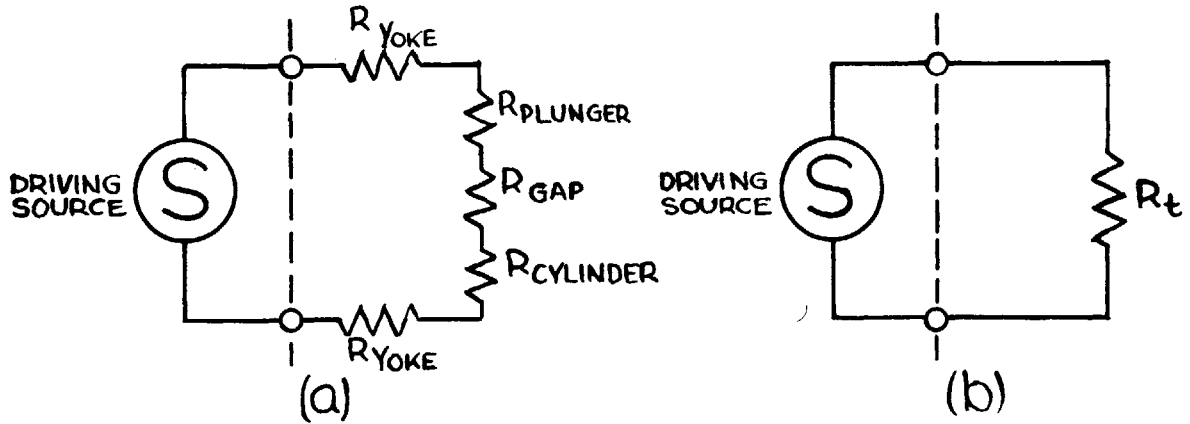


FIGURE 4

In Figure 4b the permanent magnet is represented as the driving source S and the soft-iron parts plus the air gap appear as the total external reluctance  $R_t$ . The theoretical justification for considering the permanent magnet as a driving source stems from the fact that inside the magnet the direction of the magnetizing force  $H$  is in the negative direction of the flux density  $B$ , whereas for the remaining iron and air parts  $B$  and  $H$  are both positive in the same direction. This situation then permits satisfying the necessary condition that the line integral of  $H$  around the closed path of a  $B$ -line vanishes. Now consider the source  $S$  and the external reluctance separately as shown in Figure 5.

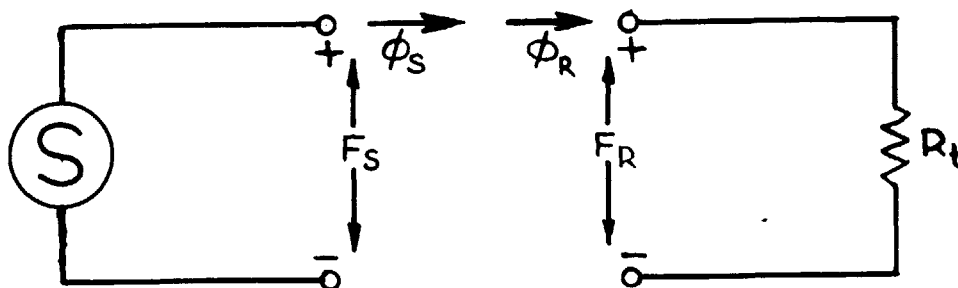


FIGURE 5

Each of the two circuit elements has a certain flux-mmf characteristic. The solution of the problem is obtained from the requirement that the two conditions

$$\phi_S = \phi_R \text{ and } F_S = F_R \dots \dots \dots (2a, b)$$

must be simultaneously satisfied. Thus by plotting the  $\phi - F$  characteristics of both the external circuit and the permanent magnet on one pair of axes the solution of the problem is obtained as the intersection of these two characteristics. The  $\phi - F$  curve of the external circuit for any fixed instant of time is obtained by adding together the mmf-drops for each part of the external circuit at selected values of flux. Figure 6 shows these curves for  $\omega t = 0, 45^\circ$  and  $315^\circ, 90$  and  $270^\circ, 135$  and  $225^\circ, 180^\circ$ , where flux is plotted vs. mmf-drop.

The  $\phi - F$  characteristic of the permanent magnet is derived from the demagnetization curve and incremental permeability for Alnico V, the cross-sectional area and length of the magnet.

In Figure 6 the curve a b c d is the normal demagnetization curve of the permanent magnet where flux is plotted vs. mmf-rise. If the magnet is magnetized to complete saturation with the plunger in the position of minimum air gap, the operating point upon removal of the external magnetizing force is represented by point (b) (Fig.6). When the plunger is moved in a direction to increase the air gap, the operating point moves along the demagnetization curve from (b) to (c) where point c represents the condition of maximum air gap. When the plunger is now returned to the

FIGURE 6

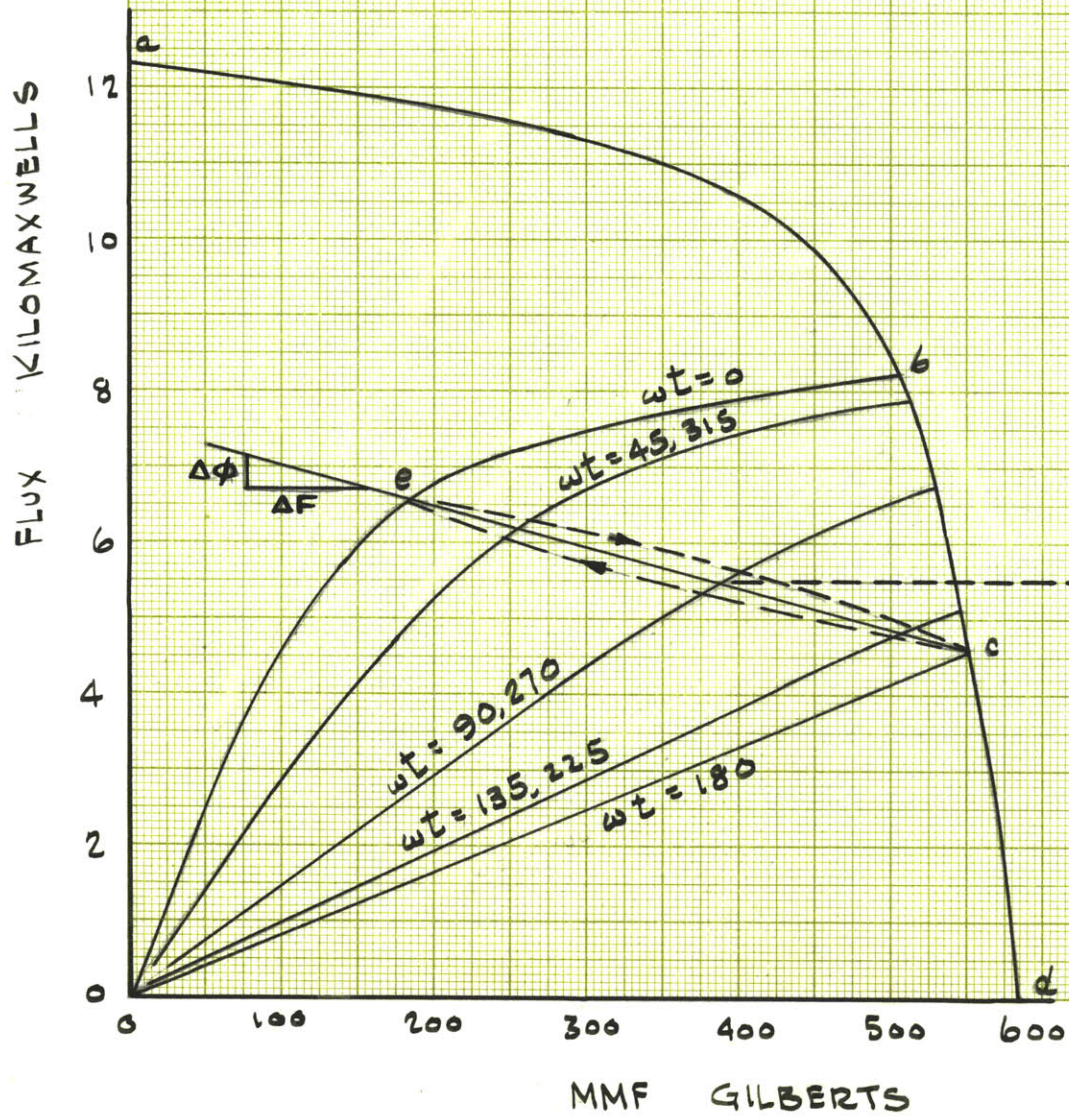
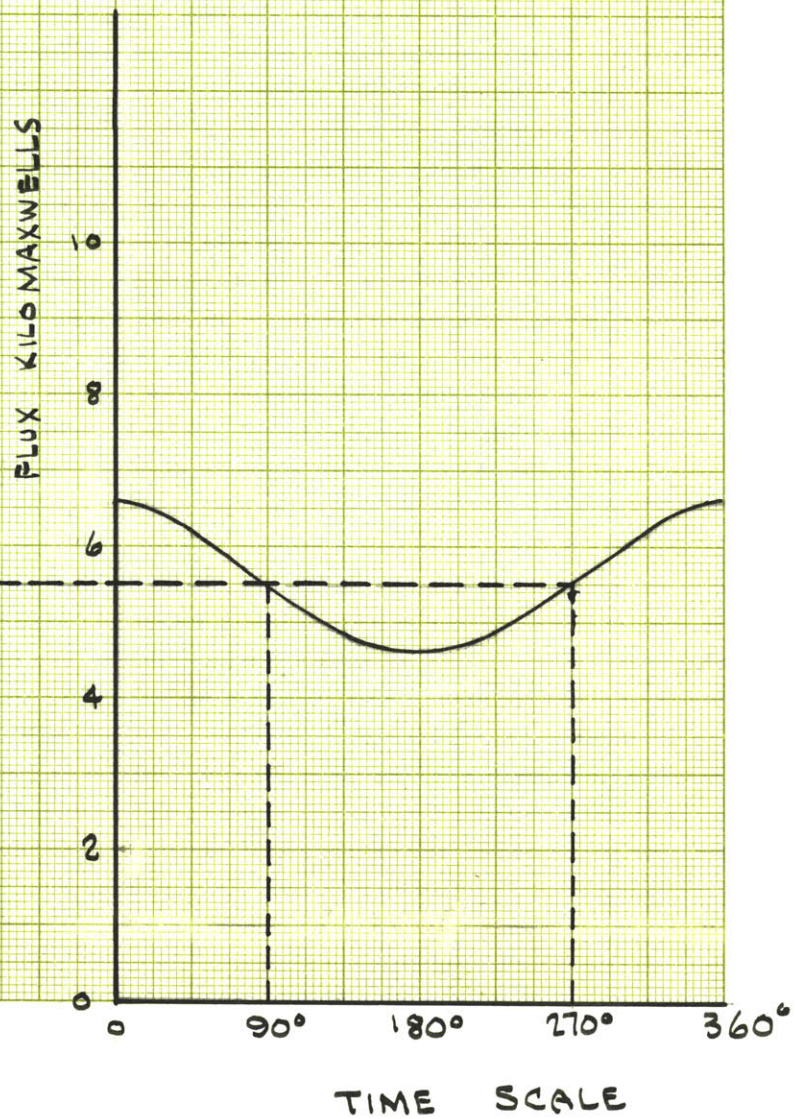


FIGURE 7



minimum air gap position, the operating point travels along the lower branch of the minor hysteresis loop (shown in dashed lines) from (c) to (e). When the air gap is increased again the operating point moves along the upper branch of the minor hysteresis loop from (e) to (c). Further periodic displacement of the plunger will cause the operating point to traverse this minor hysteresis loop. The maximum external reluctance into which the magnet must operate determines the minor hysteresis loop which the operating point will traverse. To simplify calculation it is convenient to approximate the minor hysteresis loop by a straight line connecting the tips of the loops as shown in Figure 6. This straight line is sometimes referred to as recovery line. The slope of the recovery line is proportional to the incremental permeability  $\mu_{\Delta}$  ( $\frac{\Delta\phi}{\Delta F} = \frac{\text{area of magnet}}{\text{length of magnet}} \mu_{\Delta}$ ;  $\mu_{\Delta} = \frac{\Delta B}{\Delta H}$ ). The magnitude of the incremental permeability varies somewhat with the point on the demagnetization curve at which the recovery line originates. Numerical values for the demagnetization curve and incremental permeability can be obtained from manufacturer's data<sup>1</sup>. In Figure 6 the recovery line is considered to represent the  $\phi - F$  characteristic of the permanent magnet operating into a maximum external reluctance corresponding to point C. The intersection of the recovery line with the characteristic of the external reluctance determines the flux for the time instants selected. Figure 7 shows

---

<sup>1</sup> See, for instance, The Indiana Steel Product Company, Permanent Magnet Manual No 4.



the solution of the problem where the flux values obtained from Figure 6 are plotted vs. a linear time scale.

### The Magnetic Circuit of the Alternator

In Figure 8 the alternator is drawn in a manner to emphasize the elements which are used in the symbolic representation of its magnetic circuit shown in Figure 9.

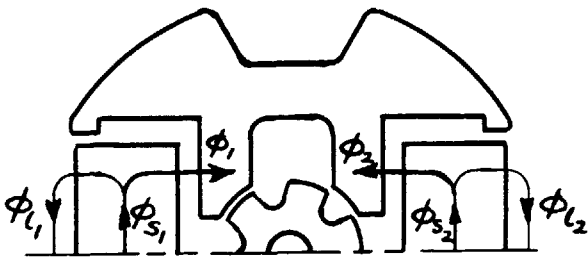


FIGURE 8

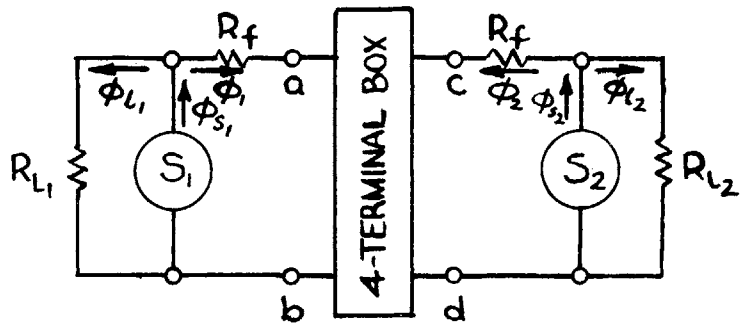


FIGURE 9

$S_1$  and  $S_2$  represent the permanent magnets,  $R_1$  and  $R_2$  the reluctance of the leakage path,  $R_f$  the reluctance of the inevitable air gap between the permanent magnet and the soft-iron structure. The 4-terminal box stands for reluctances of the stator, rotor and air gap viewed from the pairs of entry ab and cd. Leakage flux is considered here to be that fraction of the total permanent-magnet flux which is not transferred to the soft iron. It is assumed that leakage flux emanates from the "ends" of the magnet so that the flux over the effective length of the magnet is constant.

Although two identical magnets are used, their  $\phi - F$  operating characteristic is not necessarily the same, an additional requirement being that they both work into equal external reluctances. Inspection

of Figure 8, viewing from both entry pairs, shows that this requirement is satisfied for any rotor position. Consequently, the magnets exhibit identical operating characteristics and  $R_{\phi 1} = R_{\phi 2}$ . Having established this symmetry the subscripts 1 and 2 become superfluous and are subsequently omitted.

The desired solution is the flux linking the armature winding, i.e. the flux through the stator yoke. Since the stator yoke is part of the circuit, represented by the 4-terminal box, the yoke flux will be known when the relationships for the box are established. Subsequently each circuit element is considered by itself and its  $\phi - F$  characteristic determined.

#### The 4-Terminal Box

In Figure 10 are drawn the parts for which the box is to represent the equivalent circuit. It was shown in the previous article that the fluxes entering at locations a and c are equal and consequently the fluxes leaving at b and d are equal to each other and to the fluxes entering. The flux  $\phi$  entering at a has two possible paths, (1) through the upper stator yoke, (2) through the left leg towards

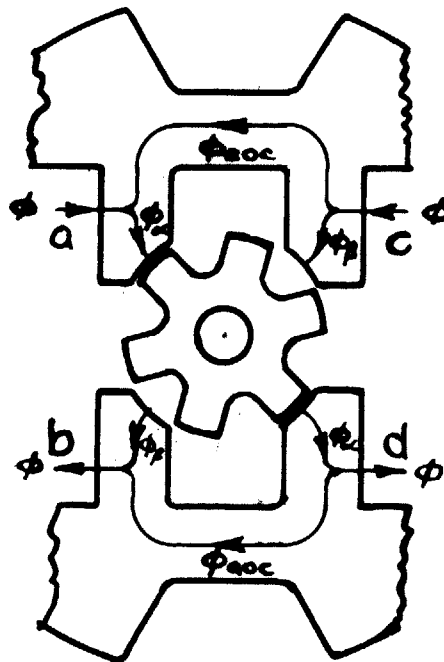


FIGURE 10

the rotor. Let the flux along the latter path be  $\phi_{\alpha}$ . Similarly, the flux entering at c has a path through the upper stator yoke

and along the right leg towards the rotor. Let the flux through the right leg be  $\phi_\beta$ . From the symmetry of the arrangement it follows that the flux in the lower right stator leg away from the rotor is equal to  $\phi_\alpha$ , while the flux through the lower left stator leg away from the rotor equals  $\phi_\beta$ . If the flux through either stator yoke is denoted by  $\phi_{a_{oc}}$  in the direction indicated in Figure 10, there follows

$$\phi_\alpha + \phi_\beta = 2\phi \dots \dots \dots (3)$$

$$\phi_{a_{oc}} = \phi_\alpha - \phi = \phi - \phi_\beta \dots \dots (4)$$

Figure 2a shows the rotor in a position where the center line of a rotor pole lines up with the center line of the upper left stator pole. Let this position be  $\theta = 0$  where  $\theta$  is the electrical angle between the center lines measured positive for a clockwise rotation of the rotor. 360 electrical degrees correspond to a rotation through a tooth-slot combination or a sixth of a mechanical revolution.

To determine the  $\phi - F$  characteristic of the box the following assumptions are made:

- (1) The stator iron is not saturated and consequently the mmf-drop in this part can be neglected compared to the mmf-drop across the air gap.
- (2) The rotor core is not saturated and can, as a first approximation, be considered as a body of constant magnetic potential.
- (3) For the purpose of calculating the air-gap permeances

the iron boundaries facing the gap may be considered as equal potential surface.

The arrangement of Figure 10 (rotor position  $\theta = 0$ ) can then be represented by the equivalent circuits shown in Figure 11

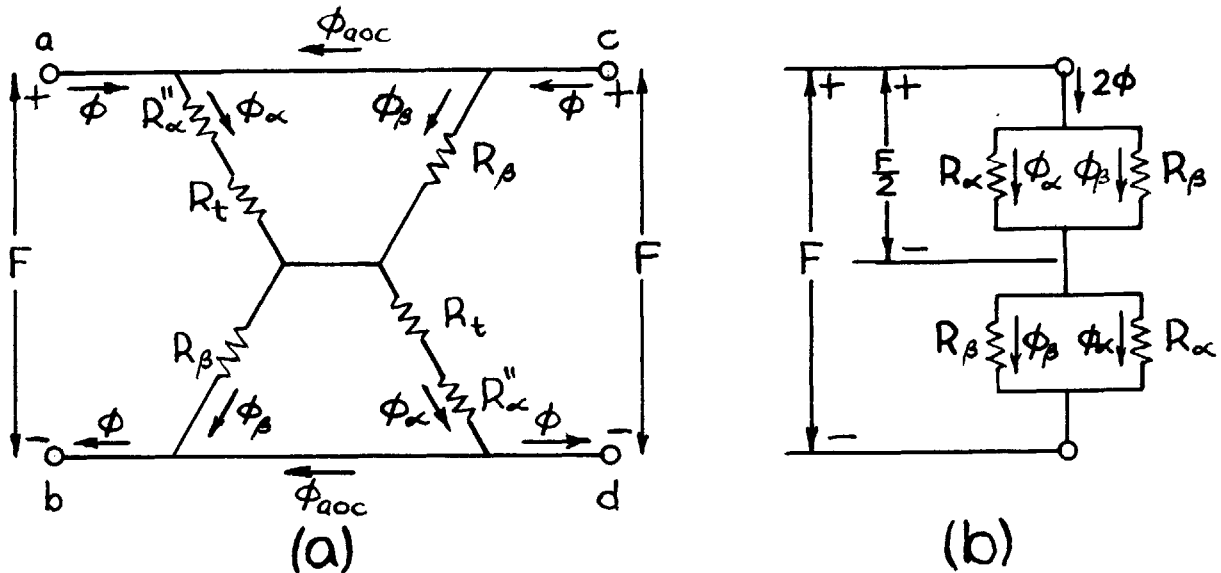


FIGURE 11

where

$R_{\alpha}''$  is the reluctance of the air space between the upper left stator pole and the rotor (also of the diametrically opposite air space).

$R_t$  is the reluctance of the rotor tooth.

$R_{\beta}$  is the reluctance of the air space between the upper right stator pole and the rotor (also of the diametrically opposite air space), and

$$R_{\alpha} = R_{\alpha}'' + R_t.$$

The fact that the reluctances of diametrically opposite parts are equal follows from the symmetry.

The next step in the solution is the determination of the air-path reluctances. The calculation of the permeance of flux paths through air between surfaces of high-permeability material

has been treated by many writers for several decades. Consequently a large number of methods evolved. At the beginning of the century F.W. Carter determined by conformal mapping the air-path permeance for an iron core with rectangular slots of width  $s$  separated from a continuous iron surface by an air gap  $g$  (see Fig.12).

The depth of the slots was assumed sufficiently large so that the bottom face had no effect on the field. He found that the permeance per cm of length for the gap and the slot over the width  $s$  is given by

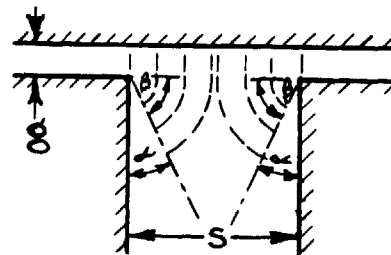


FIGURE 12

$$P = \frac{s}{g} + \frac{2}{\pi} \ln \left\{ 1 + \left( \frac{s}{2g} \right)^2 \right\} - \frac{2}{\pi} \frac{s}{g} \tan^{-1} \left( \frac{s}{2g} \right) \quad \text{cgs units} \quad \dots (5)$$

and depends only on the ratio  $s/g$ .

The solution of a two-dimensional field problem by the theory of a complex variable is restricted to simple geometrical boundaries. When the geometrical configuration is not simple an approximation to the solution may be obtained by "field mapping" or "relaxation procedures". With experience and effort these methods will furnish a closely approximating solution in most cases. Another, less time-consuming method is to calculate the permeances of probable flux paths.<sup>2</sup> Previous experience from simpler cases and the characteristic of a magnetic field to arrange itself for maximum permeance are the guiding principles in determining simple, though probable flux paths. Based on the last method, Pohl<sup>3</sup> developed a procedure to determine the

<sup>2</sup> For a detailed discussion see H.C. Roters "Electromagnetic Devices" Chap. V, John Wiley & Sons, Inc., New York.

<sup>3</sup> Robert Pohl, "Theory of Pulsating-Field Machines," JIEE (London), vol. 93, part II, p. 37, 1946.

air-path permeance, which he calls "Substitute-Angle Method". This method applies well to inductor alternators and will be used here.

In this method the path of the lines of force are assumed radial through the gap and along circle sections in the slot. For the actual slot sides fictitious-ones are substituted, which are generated by rotating the sides through an angle  $\alpha$  with the periphery as axis. To demonstrate the effectiveness and ease of the method consider the problem solved by Carter. In Figure 12 the assumed paths and the fictitious slot sides are shown in dashed lines. The gap and slot permeance per cm of length is then

$$P = 2 \int_0^{s/2} \frac{dr}{g + \beta r} = \frac{2}{\beta} \ln \left( 1 + \beta \frac{s}{2g} \right) \text{ cgs units . . . . . (6)}$$

For the large values of  $s/g$  which obtain in inductor machines Pohl recommends to operate with an angle  $\alpha = 0.47$  radian (then  $\beta = 90^\circ - \alpha = 1.1$  radians). Using this angle Pohl made a comparison between the values of permeance obtained by using Carter's formula and his own with the result that the discrepancy over the practical range of  $5 \leq s/g \leq 100$  was within one per cent. It is noted that had no substitute angle been used, the permeance values would be too small. This follows from the fact that the field naturally arranges itself for maximum permeance, and hence the substitution of artificial lines of force throughout the air space must in general lead to an underestimate of permeance.

Detailed calculations of the air-path permeances for different rotor positions using the Substitute-Angle Method are presented in Appendix I. All calculations are made per cm of active length in

the axial direction of the machine.

Figure 13 shows the solution for the open-circuit flux  $\phi_{a_{oc}}$  linking the armature winding for the rotor position  $\theta = 0$ . Referring to this figure and Figure 11, line 1 and line 2 represent the air-path reluctance corresponding to  $R_p$  and  $R_{\alpha''}$ , respectively, the abscissa being the  $\frac{F}{2}$  - scale.

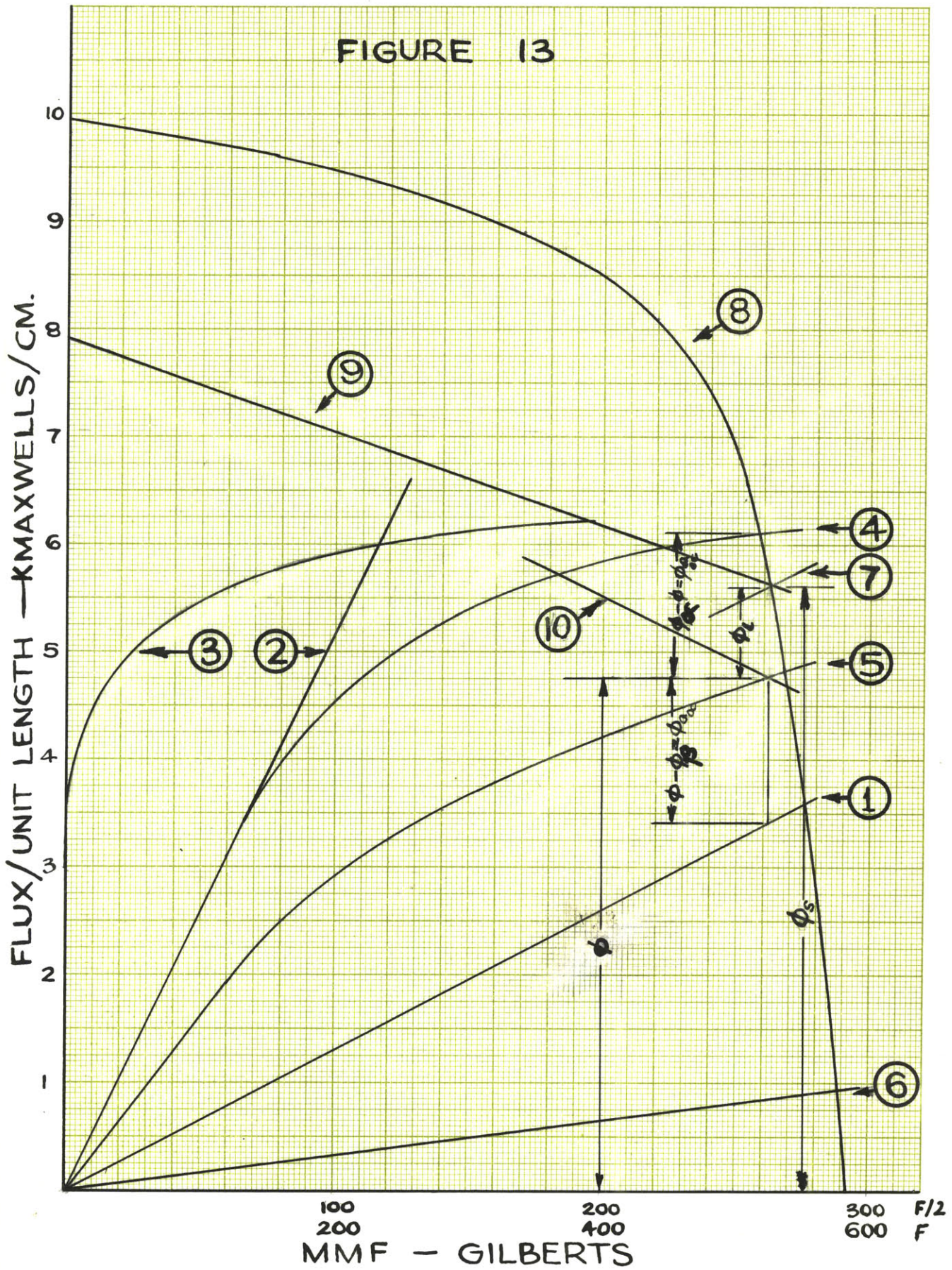
Curve 3 gives the relationship between flux per unit active length and mmf-drop for the tooth (shown as  $R_t$  in Fig.11), the abscissa is also to be read along the upper scale. This curve is obtained from the magnetization curve for the the grade of steel used in the rotor (see Appendix I). The series reluctances  $R_{\alpha''}$  and  $R_t$  are then combined to form  $R_{\alpha}$  (line 4) by adding together the mmf-drops. Next, line 1 ( $R_p$ ) and line 4 ( $R_{\alpha}$ ) are combined by adding together fluxes. One half of the resultant flux values are plotted vs. the abscissa, giving curve 5. Line 5 then is the relationship between  $\frac{\phi_{\alpha} + \phi_p}{2} = \phi$  (eq.3) and  $\frac{F}{2}$  if read on the upper abscissa scale or  $F$  if read on the lower scale. In other words, line 5 represents the  $\phi - F$  characteristic of the 4-terminal box viewed from either entry pair. Lines 4 and 5 are separated in the vertical direction by  $(\phi_{\alpha} - \phi)$ , while the distance between lines 5 and 1 equals  $(\phi - \phi_p)$ . From the construction follows  $(\phi_{\alpha} - \phi) = (\phi - \phi_p)$ . Thus equation (4) is satisfied and  $\phi_{a_{oc}}$  can be read of the graph.

Referring to Figure 9  $R_p$  is considered next. It was found by Ewing<sup>4</sup> that the equivalent air gap of "comparatively rough" joints is

---

<sup>4</sup> H.C. Roters, loc. cit. p. 86

FIGURE 13





less than 0.002". For this air gap and the contact area of the magnets the mmf-drop across  $R_t$  is negligible compared to the drops in the remainder of the circuit.

Next, consider the leakage flux from the permanent magnets, represented by the inclusion of  $R_l$  in Figure 9. The exact determination of leakage flux is a difficult problem. Sometimes a practical solution may be obtained from test. However, since the alternator can not be removed from its housing, an experimental solution is not available. In order to obtain an estimate of the order of magnitude of the leakage permeance, data given by Scott<sup>5</sup> for the open-circuit permeance of bar magnets are used. (Calculations are shown in Appendix I.) In Figure 13 the leakage permeance is represented by line 6, where the lower abscissa scale is to be used. Adding to curve 5 the leakage flux, gives line 7 which represents the total external reluctance seen by the magnet. Curve 8 is the demagnetization curve of the magnet having been completely saturated initially. The intersection of curves 7 and 8 at a establishes the operating point of the magnet. Since the magnet sees maximum external reluctance for the rotor in position  $\theta = 0$ , the recovery line originates at point a as shown by line 9. Subtracting the leakage flux from line 9 yields line 10. The desired solution is  $Oa_{oc}$  as indicated on the graph.

Having obtained a solution under the assumptions listed on page 14 one should check their validity. A total flux  $2\phi$  must be transmitted through the rotor core in the direction of decreasing magnetic potential.

---

<sup>5</sup>K.L. Scott, Magnet Steels and Permanent Magnets,  
Trans. AIEE, vol 51, pp 410-417, 1932.

For the value of  $\phi$  obtained from Figure 13 parts of the rotor core saturate, and consequently the mmf required to drive the flux through the rotor, cannot be neglected. Figure 14 shows the approximate flux density distribution in the rotor.

Core saturation is reached in the sections marked a - a. The flux through each of these sections is  $\phi$ . Denoting the reluctance of a section by  $R_c$ , the core drop is properly accounted for if in the equivalent circuit of Figure 11b the short circuit connecting the two networks is replaced by  $R_c/2$ .

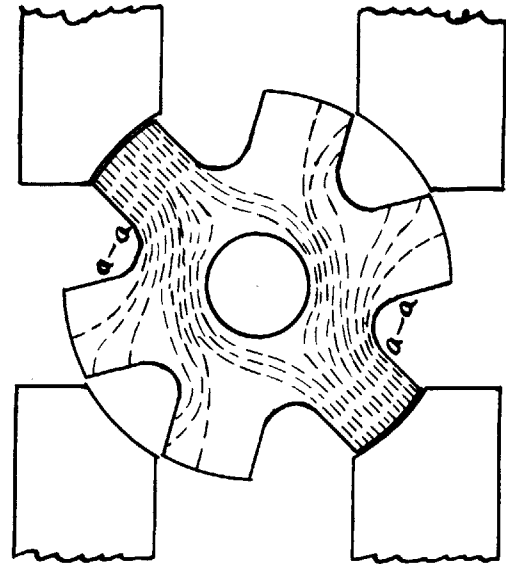


FIGURE 14

Figure 13 is modified by adding the mmf-drop for the core to line 5.

This construction is shown in Figure 15. For other rotor positions the same procedure (subject to minor changes) is used. Figure 16 shows  $\phi_{a_{oc}}$  for  $\theta = 0^\circ, 45^\circ, \text{ and } 90^\circ$ .  $\phi_{a_{oc}}$  for  $90 \leq \theta \leq 180$  is obtained from the relationship  $\phi_{a_{oc}}(90 + \theta) = -\phi_{a_{oc}}(90 - \theta)$   $0 \leq \theta \leq 90$  which follows from the fact that the roles of  $\phi_a$  and  $\phi_b$  are simply interchanged over this angle range. Careful inspection of Figure 1 will reveal that the other half wave will not be absolutely symmetrical to the first one. However, the difference is so small that it can be neglected. In Figure 17  $\phi_{a_{oc}}$  is plotted vs.  $\theta$ . If desired the wave can be expressed in a Fourier series where the coefficient would be determined

FIGURE 15

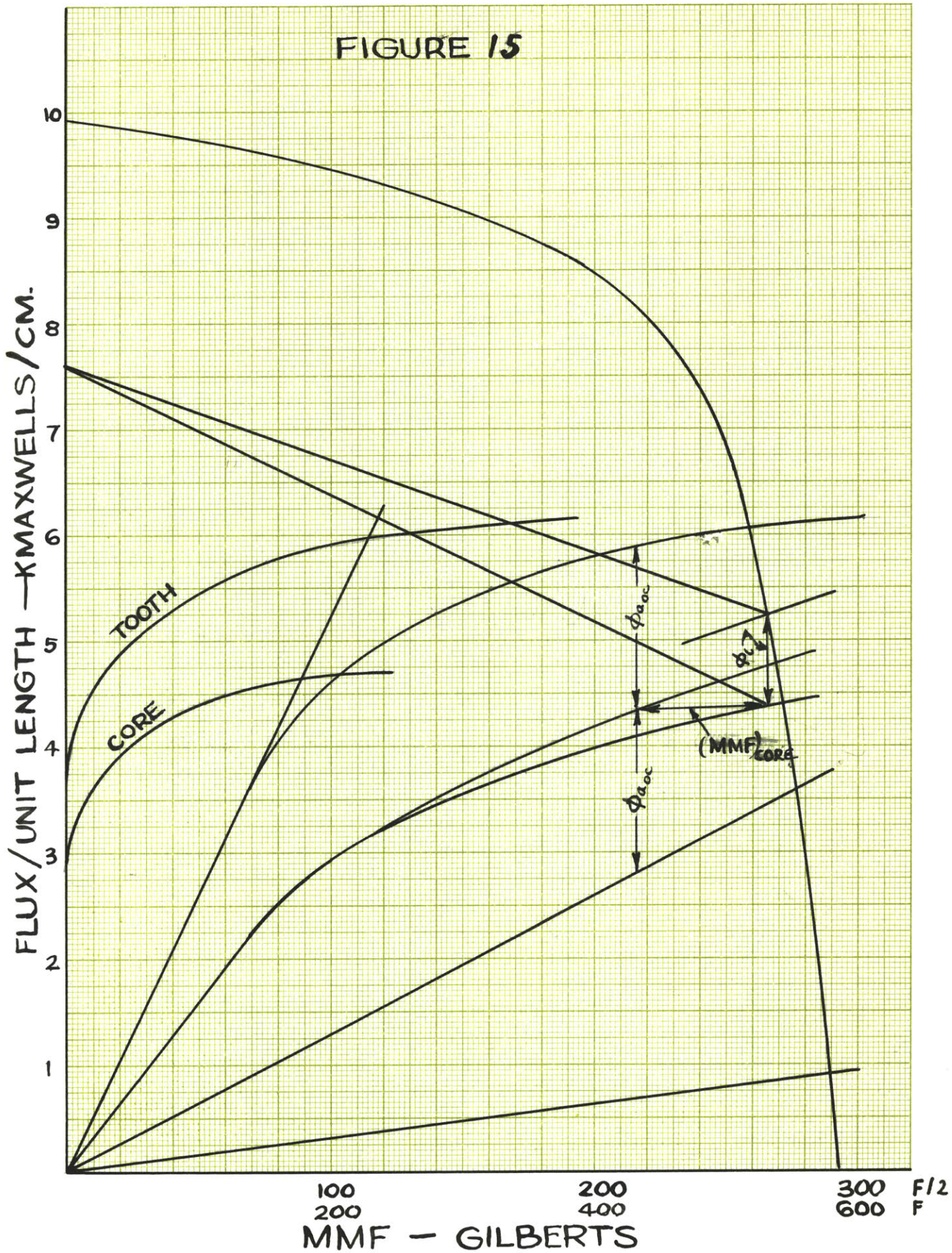
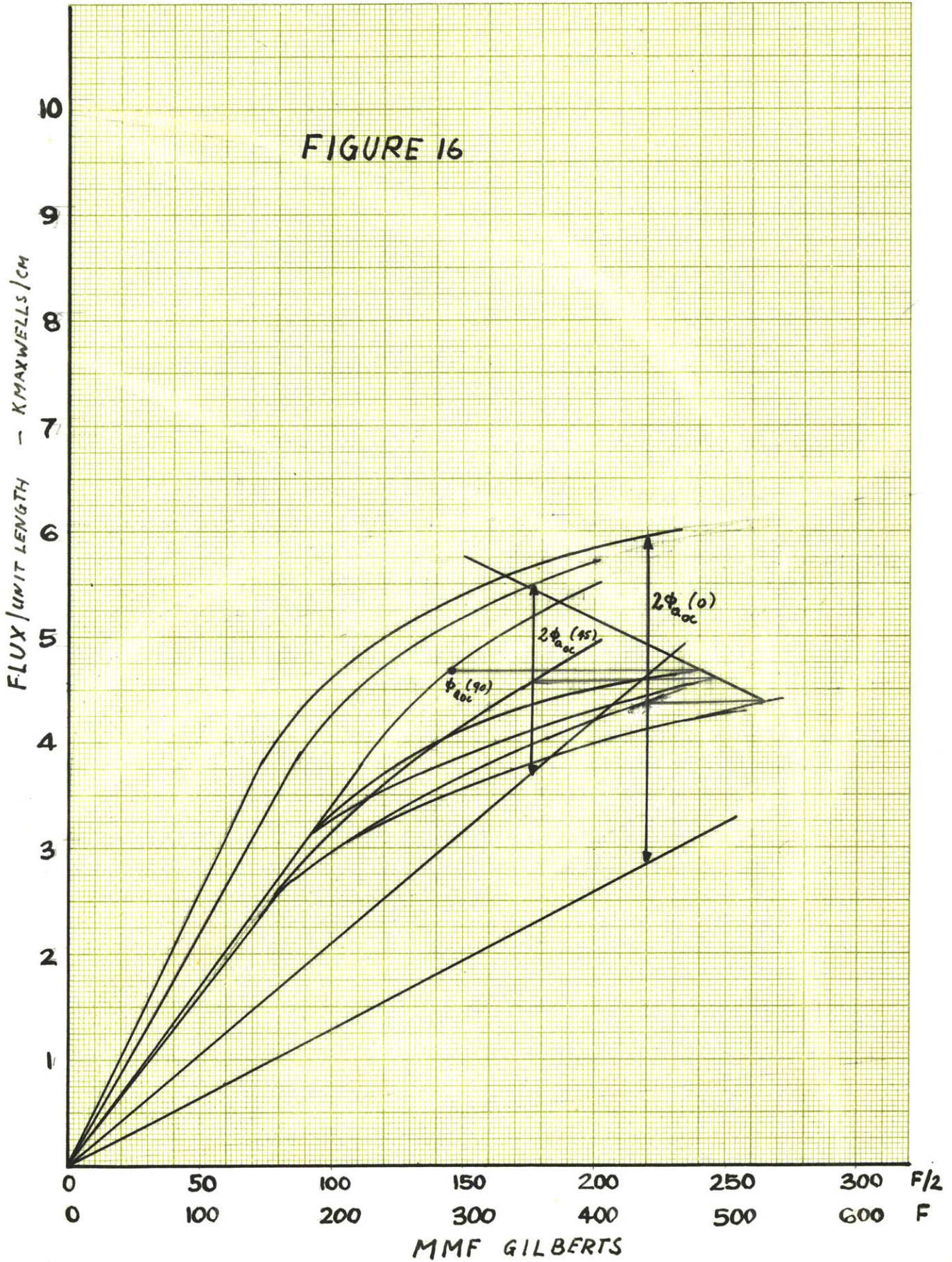
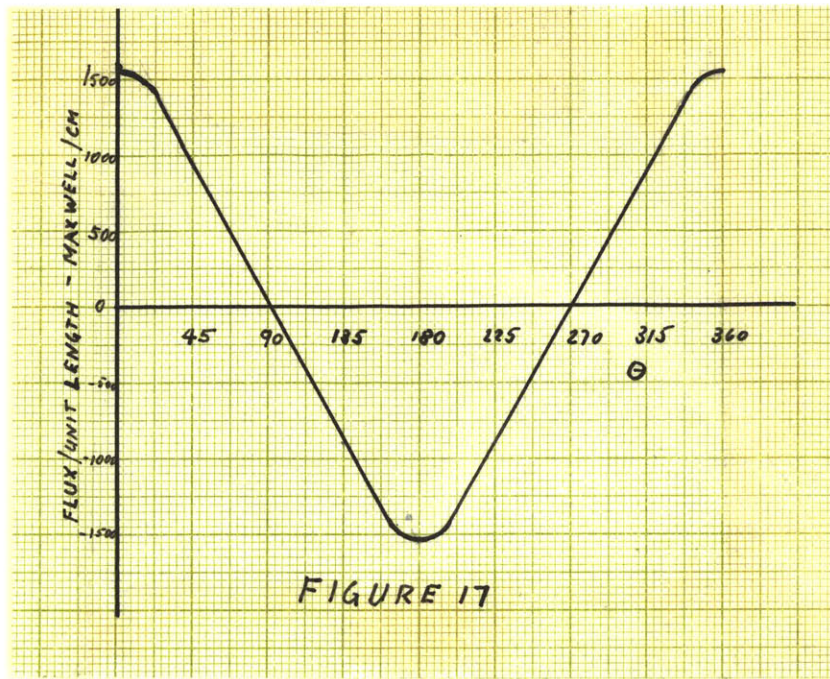


FIGURE 16





by one of the many schemes which have been devised for obtaining the Fourier expansion for a periodic function given in graphical form (e.g. Runge's method). With the assumption that the negative half wave is the mirror image of the positive half wave, the Fourier series contains only odd harmonics

$$\phi_{a_{oc}} = \sum_{n=1}^{\infty} (\phi_{a_{oc}})_n \cos(2n-1)\theta \quad \text{Maxwells/cm (7)}$$

The open-circuit voltage is given by

$$v_{oc} = N \frac{d\phi_{a_{oc}}}{dt} \cdot 10^{-8} = N \frac{d\theta}{dt} \frac{d\phi_{a_{oc}}}{d\theta} \cdot 10^{-8} \text{ Volts/cm (8)}$$

where N is the number of turns.

With the alternator operating at a mechanical speed n rpm,

$\frac{d\theta}{dt} = 2\pi \frac{n}{60} = 2\pi f$  (see eq.1 with p = 6). Consequently, the rms-value of the no-load voltage is proportional to speed (or equivalently frequency), no matter what the wave form may be.

### III. THE ALTERNATOR ON LOAD

With the alternator loaded both the permanent magnets and the windings produce magnetizing forces. The effect of the load current to change the no-load flux distribution is commonly referred to as armature reaction.

In most of the better-known high-frequency alternators<sup>6</sup>, operating on the variable-reluctance principle, the d-c ampere turns produced by the field winding and the a-c ampere turns produced by the armature winding act on the same flux path. As Pohl<sup>7</sup> showed, it is then possible to determine the flux under load by multiplying the permeance of the flux path and the sum of the d.c. and a.c. ampere turns. This method cannot readily be applied to the alternator to be considered here since the magnetomotive force produced by the permanent magnet and the ampere turns resulting from armature reaction do not act on the same path. It is therefore proposed to consider that the open-circuit condition sets the operating point and to treat armature reaction as an incremental effect with respect to this point.

Consider now the upper stator structure in Figure 1. On open circuit the entire soft-iron structure was assumed to be at a constant magnetic potential. However, with current flowing in the

---

<sup>6</sup> Several types of inductor alternators are described in a paper by J. H. Walker, High-Frequency Alternators, JIEE (London), vol. 93 part II pp 67.

<sup>7</sup> Loc. cit.

winding there is a potential difference between the parts to the right and to the left of the winding, corresponding to the number of gilberts produced by it. This potential difference causes flux to cross from one part to the other along the following paths: (1) through the upper and lower air space (also penetrating the winding) in an approximately horizontal direction, (2) through the top section of the rotor. Denoting the reluctance of path (1) by  $R_a$ , the magnetic circuit of the loaded alternator can be represented as shown in Figure 18,

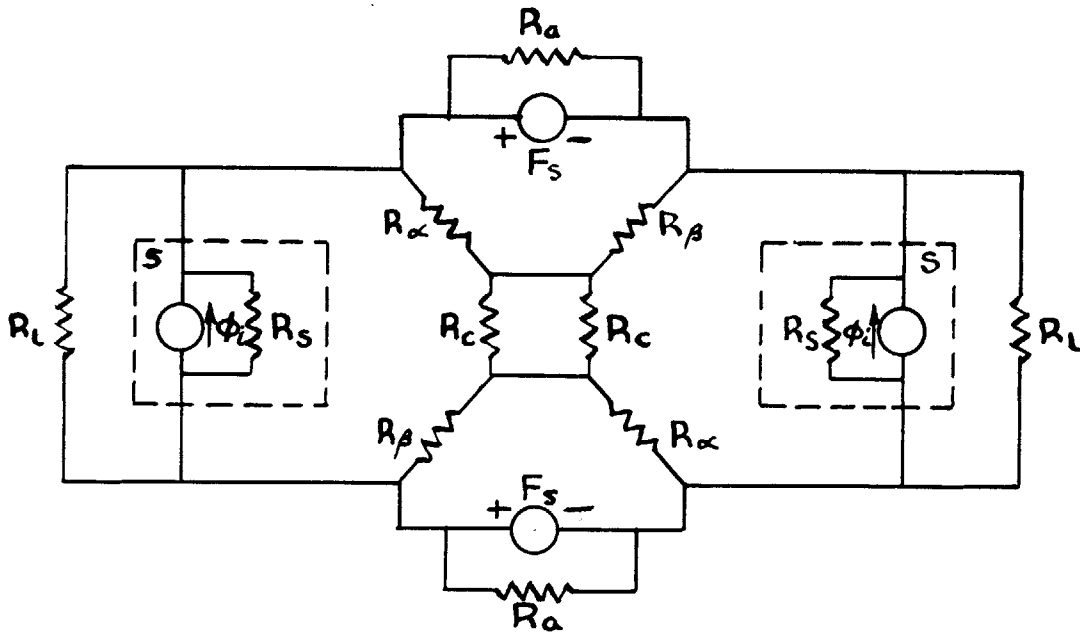


FIGURE 18

where

$R_\alpha$ ,  $R_\beta$ ,  $R_L$  are defined on page 15.

$S$  represents the permanent magnet and is shown here as an ideal flux source  $\phi_i$  in parallel with the reluctance  $R_s$ . The numerical values of  $\phi_i$  and  $R_s$  can be obtained from the straight line 9 (Fig.13) which can be represented by the equation

$$\phi = 7600 - 4.6 F. \text{ Thus } \phi_i = 7600 \text{ Maxwell/cm,}$$

$$R_s = \frac{1 \text{ Gilbert}}{4.6 \text{ Maxwell/cm.}}$$

$R_c$  is defined on page 21 and

$$F_s = 0.4 \pi Ni(t)/\text{p.u. axial length represents the mmf-source resulting from the armature current.}$$

To consider armature reaction effects, the circuit is viewed from source  $F_S$  and the incremental fluxes due to this source are determined. For the incremental analysis the ideal flux sources  $\phi_i$  are "open circuits" and reluctances are determined by  $\frac{\Delta F}{\Delta \phi}$  at the operating point of their  $\phi - F$  characteristics. Incremental reluctance will be designated by affixing a prime to the respective symbol. A rather lengthy calculation shows that the incremental fluxes through  $R_S$  and  $R_L$  are small compared to the total incremental flux. Thus as viewed from  $F_S$ ,  $R_L$  and  $R_S$  may be considered as "open circuits" without introducing appreciable error. On the other hand, the incremental flux through  $R_S$  is a measure of the magnetizing or demagnetizing force applied to the permanent magnet. Under normal operating conditions this force is sufficiently small as not to appreciably alter or displace periodically the recovery line determined for the alternator under open circuit. This is particularly true if the rotor core is saturated. However, it may happen that  $F_S$  attains abnormally high values (possibly due to an inadvertently high speed of the prime mover under capacitive load), in which case the incremental mmf applied to the magnet may cause a permanent partial demagnetization. In case one winding is accidentally open<sup>ed</sup> while the alternator is running under load, a large demagnetizing force will result and cause demagnetization.

Returning now to the conditions of normal operation when  $R_S'$  and  $R_L'$  may be considered as open circuits in respect to  $F_S$ , one realizes that  $R_C'$  has no effect on the circuit viewed from  $F_S$ .



The incremental circuit for  $F_S$  can then be represented as shown in Figure 19.

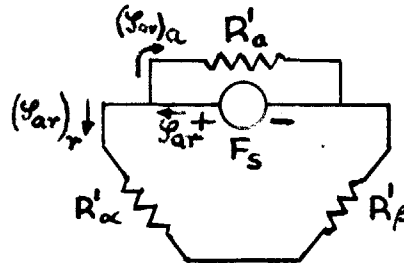


FIGURE 19

#### Determination of Armature Reaction Flux

Refer to Figure 19. In order to calculate the armature reaction flux  $\mathcal{Y}_{ar}$  for an assumed value of winding current,  $R_{\alpha}'$ ,  $R_{\beta}'$  and  $R_a$  must be known. Let us first consider  $R_a$  since its determination requires less effort than the evaluation of  $R_{\alpha}'$  or  $R_{\beta}'$ . The symbol  $R_a$  represents the reluctance offered to flux linking all or any number of winding turns having a path which is closed through air (not via the rotor). This flux is called leakage flux. Assuming that the mmf-drop in the iron is negligible against the mmf-drop in air along the leakage path,  $R_a$  is independent of the armature current. If, in addition it is assumed that the leakage flux crosses the air space in straight horizontal lines, and that the current distribution in the armature conductors is uniform, the calculation of  $R_a$  becomes straight forward. Computations for  $R_a$  are found in Appendix II. The value of the leakage permeance p.u. axial length  $P_a = \frac{1}{R_a} = \frac{.9 \text{ Maxwell}}{\text{Gilbert}} / \text{cm}$

The determination of the reluctances  $R_{\alpha}'$  and  $R_{\beta}'$  is complicated by the fact that their flux path includes saturated iron and consequently

$R_{\alpha}'$  and  $R_{\beta}'$  do not only depend on rotor position but also on the instantaneous current in the winding.

In the preceding discussion the rotor position was denoted by the angle  $\theta$  in electrical degrees. When current is considered it is convenient to introduce a time scale and to express  $\theta$  as a function of time. With the alternator operating at a constant mechanical speed  $n$  rpm this angle may be expressed as

$$\theta = \frac{2\pi n}{60} p t + \delta = \omega t + \delta \quad (9)$$

where  $t$  is time in seconds

$p = 6$  = number of rotor poles

$\omega = \frac{2\pi n}{60}$  is the electrical angular speed or frequency in radians per seconds, and

$\delta$  is the electrical angle in radians or degrees corresponding to the rotor position at  $t = 0$ .

To simplify matter, let us consider only the fundamental component of the winding current <sup>\*)</sup> and let

$$i = I_{\max} \cos \omega t \quad (10)$$

Positive current is defined as current which produces armature-reaction flux in the stator yoke from right to left, i.e. in the direction of positive (no-load) flux (see Fig.10). The significance of the angle  $\delta$  is now apparent. At the instant  $t = 0$  the center line of a rotor pole has moved  $\delta$  electrical degrees beyond the center line of the stator reference pole, while the current is at its maximum value. Consequently,  $\delta$  is the angle by which the current maximum lags the

---

\*) This situation can be approximately obtained by inserting a filter network in the load circuit.

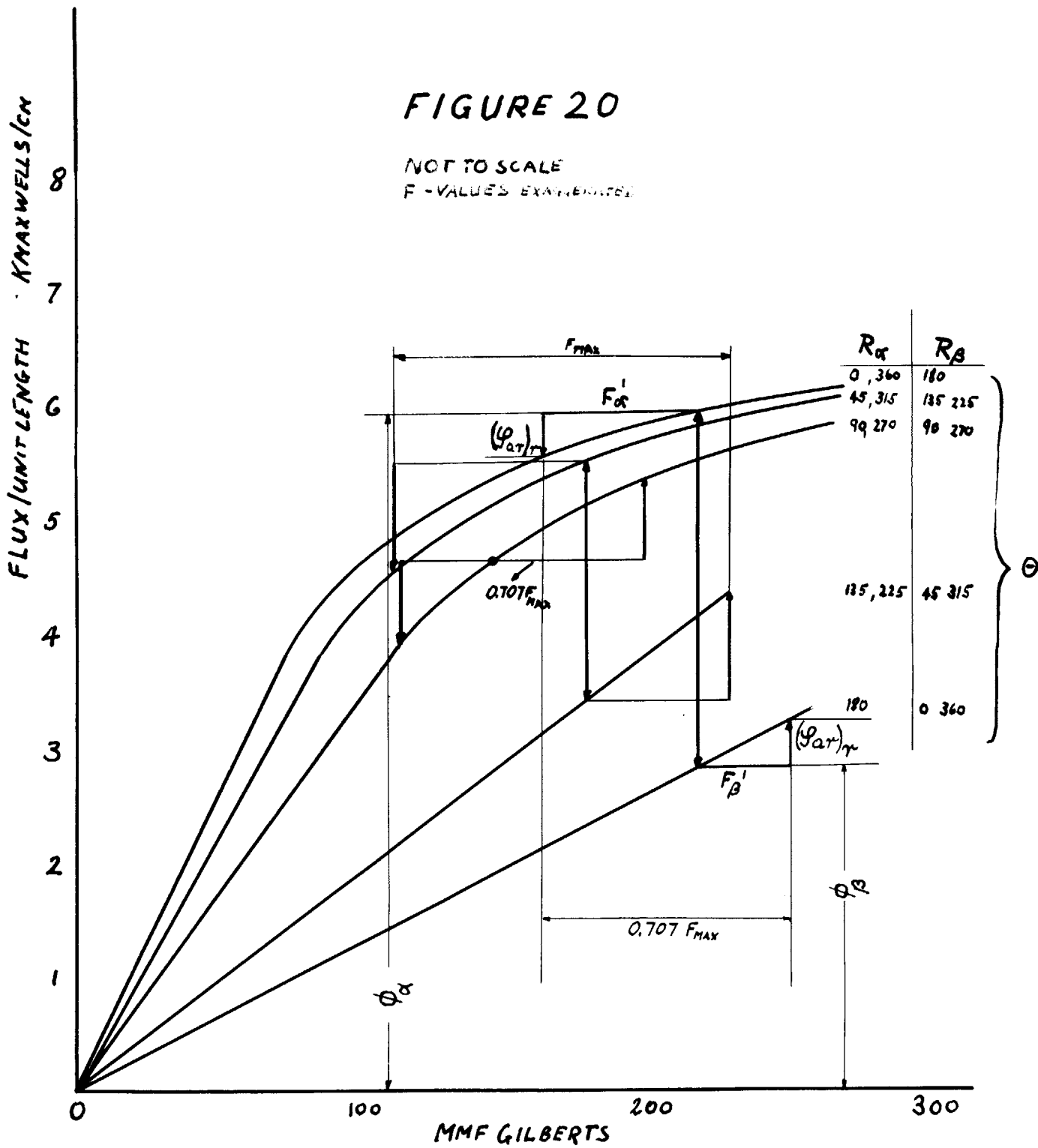
permeance maximum under the reference pole.  $\delta$  is positive for operation as a generator. The value of  $R_\alpha'$  and  $R_\beta'$  for a given rotor position  $\theta$  depends on the instantaneous current corresponding to  $\theta$ . To calculate this current value,  $I_{\max}$  and  $\delta$  must be known. It will be shown later that  $I_{\max}$  and  $\delta$  are fixed if the alternator speed and the load impedance are given. However, in order to calculate  $I_{\max}$  and  $\delta$ ,  $R_\alpha'$  and  $R_\beta'$  must be known. Under these circumstances the only practical way of calculating  $R_\alpha'$  and  $R_\beta'$  is to estimate values for  $I_{\max}$  and  $\delta$  corresponding to the specified load condition. Having obtained  $R_\alpha'$  and  $R_\beta'$ ,  $I_{\max}$  and  $\delta$  are calculated and compared with the estimated values. If necessary, this procedure may be repeated.

Let us now consider the evaluation of  $R_\alpha'$  and  $R_\beta'$  for an assumed value of  $I_{\max} = B$  amps and  $\delta = 135^\circ$ . Then  $i(t) = B \cos(\theta - 135^\circ)$  and  $F_S = 0.4\pi Ni(t) = 0.4\pi NB \cos(\theta - 135^\circ) = F_{\max} \cos(\theta - 135^\circ)$  (11)

where  $N$  is the number of turns. In Figure 16 the (static) flux-mmF characteristic of  $R_\alpha$  and  $R_\beta$  ( $\frac{F}{2}$  - scale) are plotted for  $\theta = 0, 45^\circ, 90^\circ$ . By using the relationship  $R_\beta(\theta - 180) = R_\alpha(\theta)$  and  $R_\alpha(\theta) = R_\beta(360 - \theta)$ ,  $R_\alpha$  and  $R_\beta$  can be obtained in  $45^\circ$  intervals over the entire range from  $\theta = 0$  to  $360^\circ$ . The no-load operating points are also indicated in Figure 16. These curves are redrawn in Figure 20 merely for the purpose of demonstrating the method to be used in calculating  $R_\alpha'$  and  $R_\beta'$  (numerical values will be obtained from Figure 16). For  $\theta = 0$ ,  $F_S = -0.707 F_{\max}$ . This mmF causes a negative armature reaction flux  $(\mathcal{F}_{ar})_r$  which aids the no-load flux  $\phi_r$  of the right-hand

FIGURE 20

NOT TO SCALE  
F-VALUES EXPERIMENTAL



stator pole and opposes the no-load stator flux  $\phi_a$  of the left-hand stator pole. The total ampere turns  $F_S$  are divided between the two series reluctances in such a way that equal flux increments  $(\mathcal{F}_{ar})_r$  result. The incremental reluctances are then given by

$R_{a'} = \frac{(\mathcal{F}_{ar})_r}{F_{a'}}$  and  $R_{p'} = \frac{(\mathcal{F}_{ar})_r}{F_{p'}}$ . This construction for  $\theta = 0$  is shown in Figure 20, where all components are labelled. For  $\theta = 45^\circ$ ,  $F_S = 0$ . The values of  $R_{a'}$  and  $R_{p'}$  are then determined as the slope at the operating point of the respective characteristic. For  $\theta = 90^\circ$ ,  $F_S = 0.707 F_{max}$ . The armature reaction flux is now aiding the no-load flux  $\phi_a$  and opposing  $\phi_p$ . For  $\theta = 135^\circ$ ,  $F_S$  reaches its maximum value. The incremental fluxes for each of these values of  $\theta$  are shown in Figure 20. Over the range  $180 \leq \theta \leq 360$  the events occurring for  $0 \leq \theta \leq 180$  are precisely repeated with the roles of  $R_{a'}$  and  $R_{p'}$  interchanged.

It is noted that the graphical construction of Figure 20 provides the solution for  $(\mathcal{F}_{ar})_r$  under the specified condition ( $I_{max} = B, \delta = 135^\circ$ ). There would be very little purpose in determining incremental reluctances if the alternator would always operate under this condition. This is obviously not the case and the reason for introducing incremental reluctances is to permit an analytical solution for varying operating conditions.

The incremental reluctances  $R_{a'}$  and  $R_{p'}$  can be determined from Figure 20 as a function of  $\theta$ . Defining then

$$P_{ar} = \frac{1}{R_{ar}} = \frac{1}{R_{a'} + R_{p'}} \quad (12)$$

the armature reaction flux is given by

$$(\Psi_{ar})_r = F_{max} \cos(\theta - \delta) P_{ar}(\theta) = F_{max} \cos(\omega t) P_{ar}(\omega t + \delta) \quad (13)$$

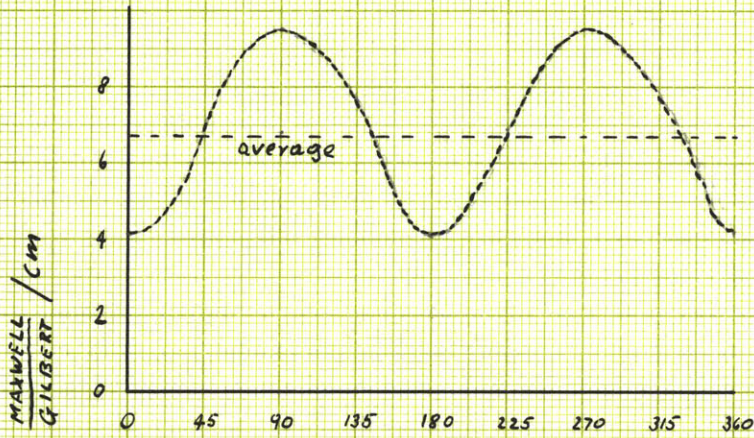
If equation (13) is used to determine  $(\Psi_{ar})_r$  for an operating condition different from the one for which  $P_{ar}$  has been calculated, an error is introduced. This error results from replacing the curved  $\phi - F$  characteristics by straight lines passing through the no-load operating point. In order to obtain a measure of this error,  $P_{ar}$  has been calculated for three largely different values of  $\delta$ , which is equivalent to considering a wide range of operating conditions.

In Figure 21 are plotted the functions  $P_{ar}(\theta)$  for parameter values of  $\delta = 135^\circ, 90^\circ, 45^\circ$ . These curves are obtained from Figure 16 by the method previously described. Referring to Fig. 21 we note that each of the three  $P_{ar}(\theta)$  functions is made up of an average term on which is superimposed a double-frequency component. Thus we may write

$$P_{ar}(\theta) = P_{ave} + \sum_{n=1} P_n \cos(n2\theta + \phi_n) \quad (14)$$

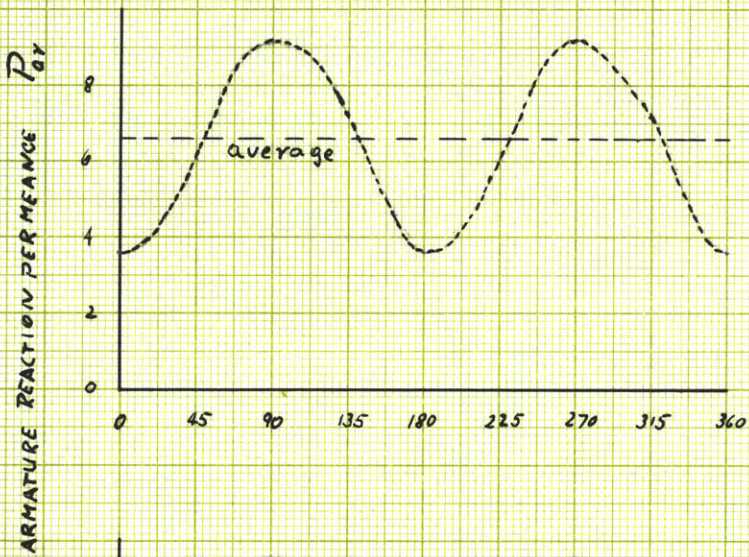
It will be shown later that for purely resistive and inductive (R-L) loads  $90^\circ \leq \delta \leq 180^\circ$  and for capacitive (R-C) loads  $0^\circ \leq \delta < 180^\circ$ . Consequently, the two top curves in Figure 21 may be considered to be representative of  $P_{ar}$  for a large variety of operating modes. Since these two curves do not differ very considerably, the error

FIGURE 21



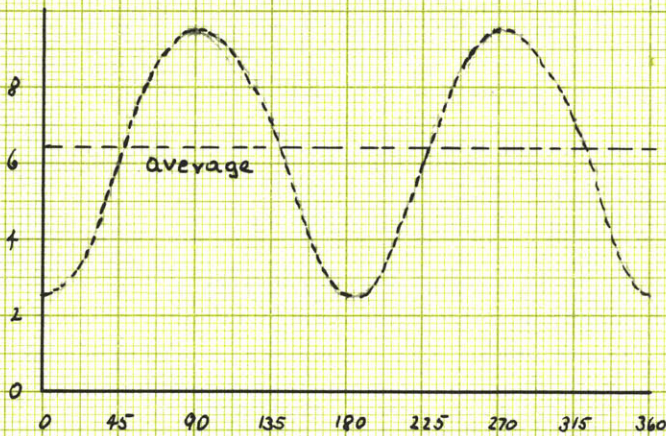
$$\delta = 135^\circ$$

$$F_{MAX} = \frac{.4\pi N I_{MAX}}{l}$$
$$= .4\pi 180 \times 0.472 / 2.2$$
$$= 58 \text{ GILBERT/CM}$$



$$\delta = 90^\circ$$

$$F_{MAX} = 58$$



$$\delta = 45^\circ$$

$$F_{MAX} = 58$$

incurred by using a fixed  $P_{ar}(\theta)$  in equation 13 for a range of alternator operating conditions seems tolerable.

In order to facilitate an analytical solution, let equation 14 be approximated by

$$P_{ar}(\theta) = P_{ave} - P_1 \cos(2\theta) \quad (15)$$

Approximating the  $P_{ar}(\theta)$ -functions of Figure 21 by equation 15 is expected to give reasonable results for rms-currents and rms-voltages. However, if the wave forms of these quantities are to be considered, curves like those in Figure 21 should be plotted, and their Fourier representation (eq.14) be used.

We are now in a position to determine the resultant flux linking the armature winding for the loaded alternator. The resultant flux is equal to the sum of the no-load flux  $\phi_{a_{oc}}$  and the armature reaction flux  $\phi_{ar}$ . Figure 17 shows the no-load flux as a function of  $\theta$ . Restricting ourselves to the fundamental component, the equation for this flux may be written as

$$\phi_{a_{oc}} = \phi_{max_{oc}} \cos\theta \quad (16)$$

where  $\phi_{max_{oc}}$  is determined by Figure 17. Referring to Figure 19 the armature reaction flux is obtained by multiplying the mmf resulting from the armature current by the sum of the constant leakage permeance  $P_a$  and the armature reaction permeance  $P_{ar}$ , hence

$$\mathcal{F}_{ar} = (\mathcal{F}_{ar})_a + (\mathcal{F}_{ar})_r = 0.4\pi N i(t) \{P_a + P_{ar}\} \quad (17)$$

Considering only the fundamental component of the current  $i(t)$  as in equation 10 and substituting for  $P_{ar}$  the value from equation 15



gives

$$\varphi_{ar} = 0.4\pi N I_{max} \cos \omega t \{ P_a + P_{ave} - P_l \cos 2\theta \} \quad (18)$$

using equation 9 and adding  $\phi_{a_{oc}}$  to  $\varphi_{ar}$  results in

$$\phi_{res} = \phi_{max_{oc}} \cos(\omega t + \delta) + 0.4\pi N I_{max} \cos \omega t \{ P_a + P_{ave} - P_l \cos 2(\omega t + \delta) \} \quad (19)$$

with the trigonometric identity  $\cos \alpha \cos \beta = \frac{1}{2} [\cos(\alpha - \beta) + \cos(\alpha + \beta)]$  and letting

$$P_a + P_{ave} = P_o \quad (20)$$

$$\begin{aligned} \phi_{res} = & \phi_{max_{oc}} \cos(\omega t + \delta) + 0.4\pi N I_{max} P_o \cos \omega t \\ & - 0.4\pi N I_{max} \frac{P_l}{2} \cos(\omega t + 2\delta) - 0.4\pi N I_{max} \frac{P_l}{2} \cos(3\omega t + 2\delta) \end{aligned} \quad (21)$$

Equation 21 shows the very significant fact that even if open-circuit flux, armature current, and armature reactance permeance are assumed sinusoidal, the resultant flux will contain a third harmonic. This means, no matter how much pain is taken to shape the rotor poles for sinusoidal open-circuit voltage, harmonics will be generated under load unless other means are used to eliminate them.

For the discussion which follows, only the fundamental component of the resultant flux is considered. Then equation 21 can be represented in form of a vector diagram, as shown in Figure 22, with the current taken as reference vector.  $\phi_{res}$  induces the emf  $E$  which lags the resultant flux by  $90^\circ$ . To obtain the terminal voltage  $V$

the  $IR_{\text{eff}}$ -drop must be subtracted from  $E$  <sup>\*)</sup>, where  $R_{\text{eff}}$  is the <sup>\*\*) )</sup> effective a-c resistance of the winding.

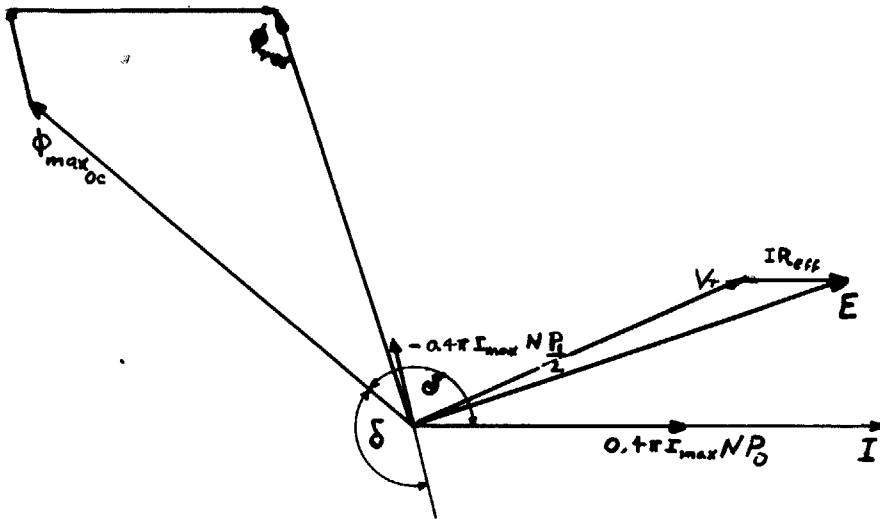


FIGURE 22

Determination of Current for Given Load and Speed

With a load impedance  $Z$  connected to the alternator terminals

$$\bar{E} = \bar{V} + \bar{I}R_{\text{eff}} = \bar{I}Z + \bar{I}R_{\text{eff}} = \bar{I}(R_{\text{eff}} + R + jX) \quad (22) \quad \text{***)}$$

with  $\bar{Z} = R + jX$  and  $X = \begin{cases} \omega L & \text{for inductive load} \\ -\frac{1}{\omega C} & \text{for capacitive load} \end{cases} \quad (23)$

\*) What is commonly known as leakage reactance has already been taken care of.

\*\*) Into the effective resistance are reflected the increase of copper loss in the winding, resulting from non-uniform current distribution and the incremental iron loss, caused by armature current.

\*\*\*) Electrical quantities without a subscript refer to rms-values.

From the vector diagram

$$\bar{\phi}_{res} = \phi_{max_{oc}} / \delta + 0.4\pi N I_{max} P_o - 0.4\pi N I_{max} \frac{P_i}{\lambda} \frac{\angle 2\delta}{\lambda} \quad (24)$$

using Faraday's Law

$$\bar{E} = -j \frac{N\omega}{\sqrt{2}} \bar{\phi}_{res} \cdot 10^{-8} \quad (25)$$

and combining equations 22, 24 and 25 yields

$$\frac{N\omega}{\sqrt{2}} \cdot 10^{-8} \phi_{max_{oc}} \frac{\angle \delta - 90}{\lambda} = I \left\{ R_{eff} + 0.4\pi N^2 \frac{P_i}{\lambda} \cdot 10^{-8} \omega \sin(2\delta) + R \quad (26) \right. \\ \left. + j(0.4\pi N^2 P_o \cdot 10^{-8} \omega - 0.4 N^2 \frac{P_i}{\lambda} \cdot 10^{-8} \omega \cos 2\delta + X) \right\}$$

letting

$$0.4\pi N^2 P_o \cdot 10^{-8} = L_o, \quad 0.4\pi N^2 \frac{P_i}{\lambda} \cdot 10^{-8} = L_1 \quad (27 \text{ a,b,c})$$

$$\frac{2\pi}{\sqrt{2}} N \cdot 10^{-8} \phi_{max_{oc}} = K$$

where the

$L_s$  have the dimensions of inductance

and  $K$  has the dimension of Volt/cps,

then equation 26 becomes

$$\bar{E} = Kf \frac{\angle \delta - 90}{\lambda} = I \left\{ R_{eff} + \omega L_1 \sin 2\delta + R + j(\omega L_o - \omega L_1 \cos 2\delta + X) \right\} \quad (28)$$

If in equation 28 the real part of the right-hand side is equated to the real part of the left-hand side, and the same procedure is followed for the imaginary parts, two independent equations in the unknowns  $I$  and  $\delta$  are obtained. Solving these equations, one finds

$$\tan \delta = - \frac{R_{\text{eff}} + R}{\omega(L_0 + L_1) + X} \quad (29)$$

$$I = \frac{Kf \sin \delta}{R_{\text{eff}} + R + \omega L_1 \sin 2\delta} \quad (30)$$

Equations 29 and 30 permit then to find the current I when the load (R and X) and the speed n (or equivalently  $\omega$  or f) are specified. We note from equation 29 that  $90^\circ < \delta < 180^\circ$  for inductive loads, since then  $X > 0$  and  $\tan \delta < 0$ . For capacitive loads for which  $X < 0$  :  $90^\circ < \delta < 180^\circ$ ,  $0 < \delta < 90^\circ$ ,  $\delta = 0$  if the denominator of equation 29 is positive, negative, zero, respectively.

Although equations 29 and 30 permit to solve for the current, it may be more helpful to use an equivalent circuit representation. For this purpose equation 28 is best adapted and is used to obtain the circuit shown in Figure 23.

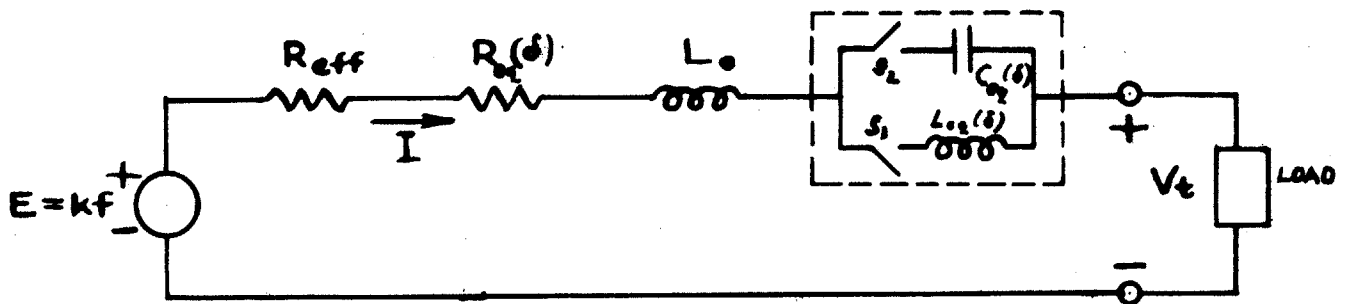


FIGURE 23

Where

$$R_{eq}(\delta) = \omega L_1 \sin 2\delta \quad \text{and is } \begin{cases} \text{positive for } 0 < \delta < 90 \\ \text{negative for } 90 < \delta < 180 \end{cases}$$

$$L_{eq}(\delta) = \omega L_1 \cos 2\delta$$

$$\frac{1}{C_{eq}(\delta)} = \omega^2 L_1 \cos 2\delta$$

switch  $S_1$  is closed ( $S_2$  open) when  $45 < \delta < 135$

switch  $S_2$  is closed ( $S_1$  open) when  $0 < \delta < 45, 135 < \delta < 180$

Numerical values for the circuit parameters are obtained from figures 17 and 21 in conjunction with equations 20 and 27, and the value of leakage permeance given on page 28. With the number of turns  $N = 180$  and an effective axial length  $l = 2.2$  cm

$$\left. \begin{aligned} K &= \frac{2\pi N}{\sqrt{2}} 10^{-8} \phi_{\max_{oc}} = \frac{2\pi}{\sqrt{2}} 180 \cdot 10^{-8} \cdot 1550 \cdot 2.2 = 0.0274 \text{ V/cps} \\ L_0 &= 0.4\pi N^2 P_0 10^{-8} = 0.4\pi (180)^2 \cdot 7.6 \cdot 2.2 \cdot 10^{-8} = 6.8 \text{ mh} \\ L_1 &= 0.4\pi N^2 \frac{P_1}{2} 10^{-8} = 0.4\pi (180)^2 \cdot \frac{2.7}{2} \cdot 2.2 \cdot 10^{-8} = 1.2 \text{ mh} \end{aligned} \right\} 31$$

The usefulness of this equivalent circuit is impaired by the fact that the circuit elements having the subscript "eq" are dependent on the load, i.e. are non-linear. It is noted that only  $L_1$  gives rise to these non-linear elements. The value of  $L_1$  is always less than  $\frac{L_0}{2}$ , and is usually small compared to  $L_0$ . If it is assumed that the effect of  $L_1$  on the fundamental component of the resultant flux is negligible, (i.e. the quantity  $0.4\pi I_{\max} \frac{P_1 N}{2}$  in the

vector diagram of Figure 22 is discarded) the simple equivalent circuit shown in Fig.24 is obtained. The element values of this

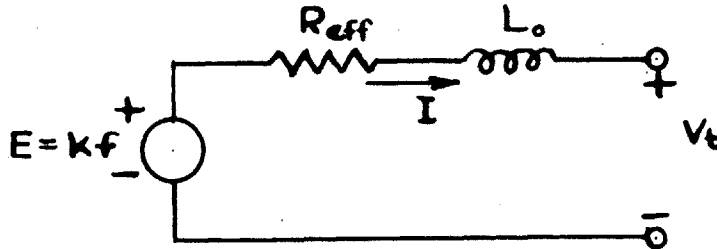


FIGURE 24

equivalent circuit can be determined from design data of the alternator as was done previously or may be obtained from simple tests. The value of K is found from an open-circuit test as the ratio of the no-load voltage to the frequency, or

$$K = \frac{V_{oc}}{f} \quad (32)$$

A short-circuit test will determine the value of  $L_0$ . The output terminals are short-circuited through a thermoammeter, and the alternator is driven at a sufficiently high speed, so that  $\omega L_0 \gg R_{eff}$ . This condition can be observed experimentally by the fact that a constant current will result above a certain frequency. Denoting this value of current by  $I_{sc}$ ,

$$L_0 = \frac{K}{2\pi I_{sc}} \quad (33)$$

In case  $I_{sc}$  is of such magnitude as to be destructive, the procedure is altered by connecting a known inductance  $L_n$  across the output,

just sufficient to limit the current to a safe value  $I_{sc}'$ , then

$$L_o = \frac{K}{2 \pi I_{sc}'} - L_n \quad (32a)$$

The effective resistance  $R_{eff}$  is discussed in the following chapter where the performance characteristics of the alternator are calculated from the equivalent circuit of Figure 24 and compared with experimental results.

#### IV. TEST RESULTS AND THEIR COMPARISON WITH THE THEORY

Before the experimental results are presented a few preliminary remarks seem necessary. After receiving the alternator, the rotor was removed in order that parts of the machine could be inspected. The removal of the rotor and the fact that the polarities of the magnets are in opposition cause each magnet to operate on a portion of its demagnetization curve corresponding to small values of flux density. Consequently, when the machine is reassembled the permanent magnets will not reassume their initial state and should be recharged. At the time, the author did not have a suitable electromagnet at his disposal. Therefore the machine was given to a local company having a "large" electromagnet with instructions to magnetize the permanent magnets. When the alternator was returned the test results presented in this chapter were obtained. Later the author built an electromagnet capable of supplying sufficient ampere turns to yield saturation flux density in the permanent magnet. Having charged the permanent magnets with this electromagnet, the alternator was given an open-circuit test. While taking data of no-load voltage vs. frequency, a number of turns of one winding became permanently short circuited due to an unknown cause. The data already obtained showed that the no-load voltage was much higher ( $K=0.029$  V/cps) than for the case where the magnets had been polarized by the above-mentioned company, indicating that they did not fully charge the magnets.

In the previous chapters all curves and numerical calculations were derived under the assumption that the magnets have been



originally charged to their saturation value, as would normally be the case. Since the test results that follow were not obtained for this condition, the equivalent circuit values given on page 40 do not apply. In order to compare experimental and calculated results the equivalent-circuit elements must be evaluated for the state of the permanent magnets under which the tests were taken. This is accomplished by determining the value of the equivalent-circuit elements from experimental data. For all tests the alternator was driven by its own turbine, operated on filtered air (the alternator and turbine were supplied as a unit), and the two stator windings were connected in parallel. Voltage and current were measured with thermo-couple instruments, and frequency with an electric<sup>an</sup> frequency meter. In the following the results from experimental tests are presented and discussed, data and sample calculations are shown in Appendix III, where also the equivalent circuit used for calculations is derived. In all calculations involving the equivalent circuit, the effective armature resistance was taken equal to the d-c resistance of the winding. It is known that this results in a value which is too small. The increase in a-c resistance, resulting from non-uniform current distribution in the winding can be estimated by using a formula<sup>\*)</sup> developed for coils embedded in slots. According to this formula the per-cent increase of

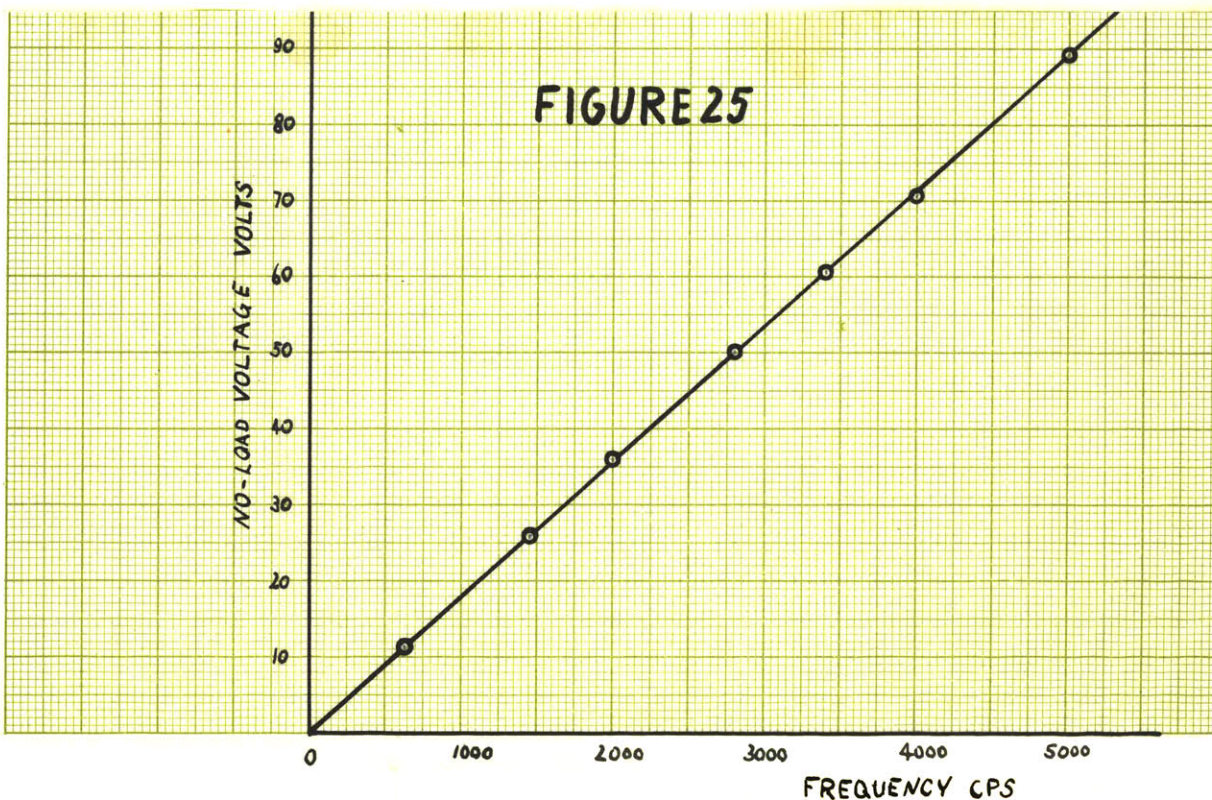
---

\*) See e.g. Rudolf Richter, Kurzes Lehrbuch der elektrischen Maschinen, p 94, Springer-Verlag 1949

resistance varies approximately with the square of the frequency. A rough calculation shows that for the small wire size of the alternator winding the increase in resistance from this cause will not exceed 10 per cent for frequencies up to 8 kcps. On the other hand the increase in effective resistance due to incremental core loss, which appears to be of much larger order of magnitude (200 to 400 per cent at 8 kcps), is much more difficult to account for. It is suggested that the effective resistance be determined experimentally. A possible procedure will be mentioned when test results with a capacitive load are considered.

#### Open-Circuit Characteristic

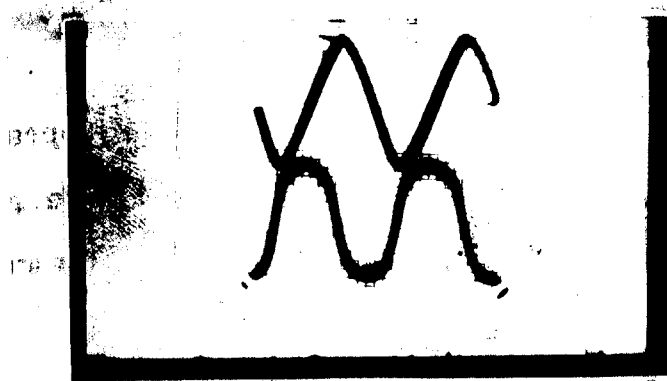
Figure 25 shows the no-load voltage to be a linear function of frequency. This was to be expected from the considerations on page 24, if the change of apparent permeability due to core loss is neglected.



The slope of this straight line gives the value of K.

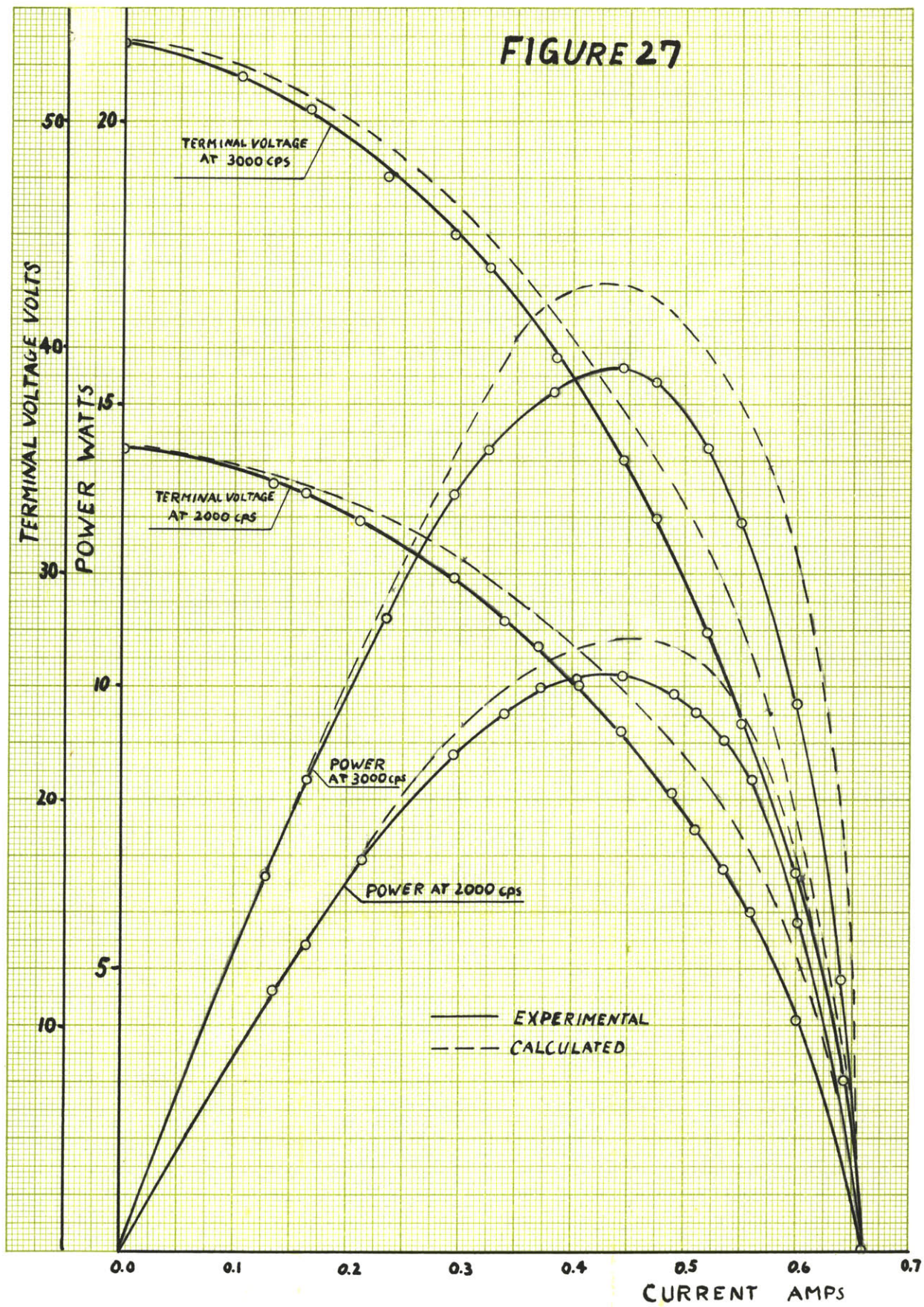
$$K = 0.0178 \text{ Volt/cps.}$$

The top and bottom curves of Figure 26 represent the no-load flux and open-circuit voltage, respectively, as they appeared on the oscilloscope. The flux pattern was obtained by using an integrating circuit.



#### Resistive Load

In Figure 27 the curves in full lines show the output power and terminal voltage as a function of load current for a purely resistive load at a fixed frequency. Two sets of curves are shown, one for a frequency of 2000 cps, the other for 3000 cps. Calculated results are shown in dashed lines. It is observed that maximum power for both the 2000 cps and 3000 cps curve occur at approximately the same current. This result can also be obtained by considering the equivalent circuit. For a fixed frequency the internal impedance of the alternator is constant. Maximum power transfer to the load then results when the load



resistance matches the magnitude of the internal impedance, or

$$R = \sqrt{R_{\text{eff}}^2 + (\omega L_0)^2}$$

and

$$I = \frac{Kf}{\sqrt{(R_{\text{eff}} + R)^2 + (\omega L_0)^2}}$$

For  $\omega L_0 \gg R_{\text{eff}}$ ,  $R \approx \omega L_0$  and

the current at which maximum power occurs

$$I \approx \frac{Kf}{\sqrt{2} \omega L_0} = \frac{K}{\sqrt{2} 2\pi L} \approx \frac{1}{\sqrt{2}} I_{\text{sc}}$$

and is independent of frequency.

Figure 28 shows current wave forms for a resistive load of 80 ohms at 3 different frequencies. The top curve corresponds to  $f = 5000$  cps and  $I = .53$  amp, the one below it to  $f = 2000$  cps and  $I = .34$  amp and the one on the bottom was taken for  $f = 500$  cps and  $I = .101$  amp. The effect of armature reaction on the wave form as current increases, is clearly recognized.

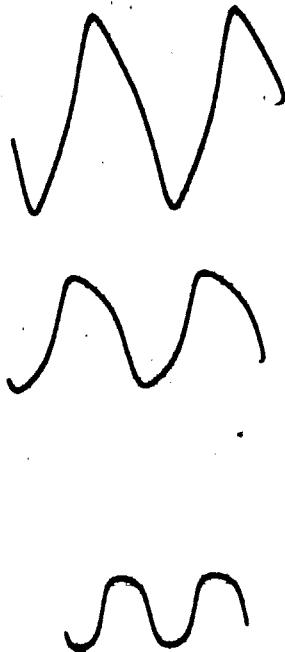


FIGURE 28

### Capacitive (R-C) Load

Figures 29, 30, 31, 32 show the current, voltage across the capacitor, terminal voltage, and power, respectively, as a function of frequency for a series R-C load. Three curves are shown in each figure, corresponding to resistance values of 30, 50, and 100 ohms. The same capacitance was used throughout this test, and its value was selected to produce a reactance equal in magnitude to the reactance resulting from the equivalent-circuit inductance at 2000 cps. In Figure 29 calculated values are shown along with the experimental results. Comparing the experimental with the calculated values, one finds that the discrepancy is largest for frequencies in the vicinity of 2000 cps. Also the discrepancy increases with decreasing load resistance. At frequencies close to 2000 cps. the current calculated from the equivalent circuit depends almost entirely on  $(R_{\text{eff}} + R)$ , since the resultant reactance is approximately zero. Consequently, the value of  $R_{\text{eff}}$  exerts an appreciable influence on the equivalent circuit behavior over this frequency range. If for  $R_{\text{eff}}$  a larger value than  $R_{\text{dc}}$  had been used (which would be the proper procedure), the discrepancy between experimental and calculated results would be smaller.

Under the assumption that the equivalent circuit of Figure 24 is a proper representation of the alternator, the remarks made in the preceding paragraph suggest a possible experimental procedure to determine  $R_{\text{eff}}$  as a function of frequency: The alternator is driven at a speed corresponding to a frequency  $f_1$ , operating into

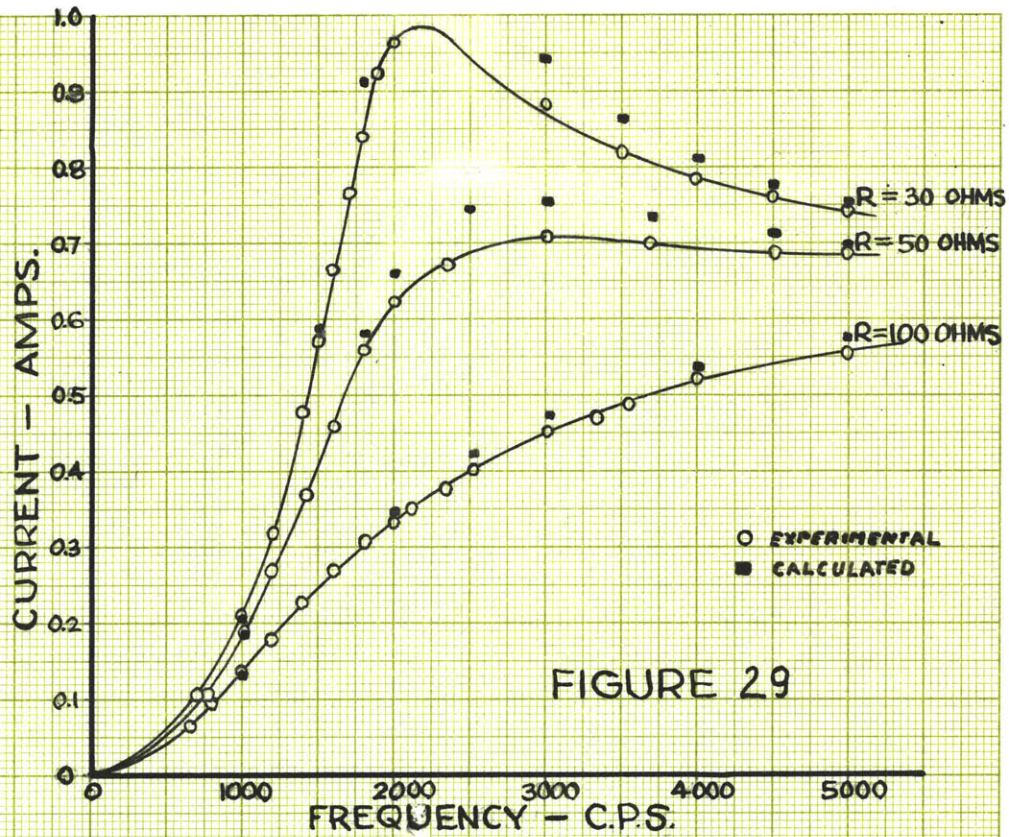


FIGURE 29

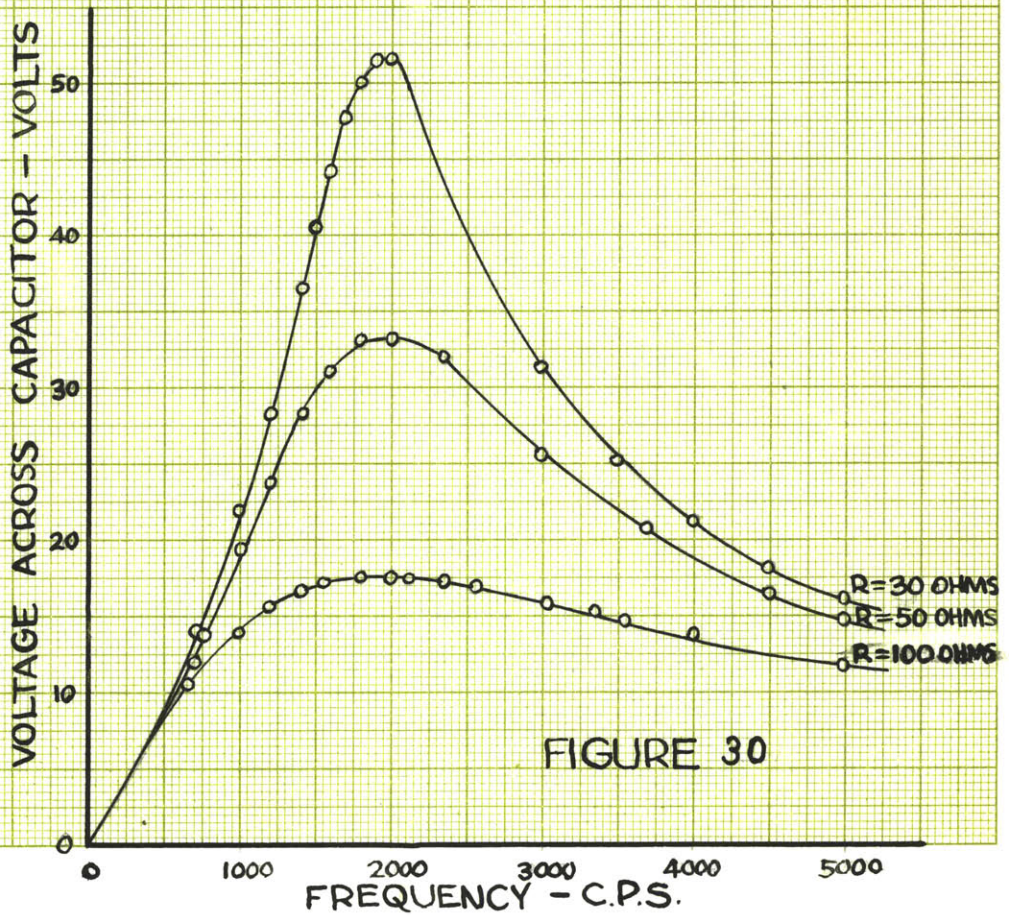


FIGURE 30

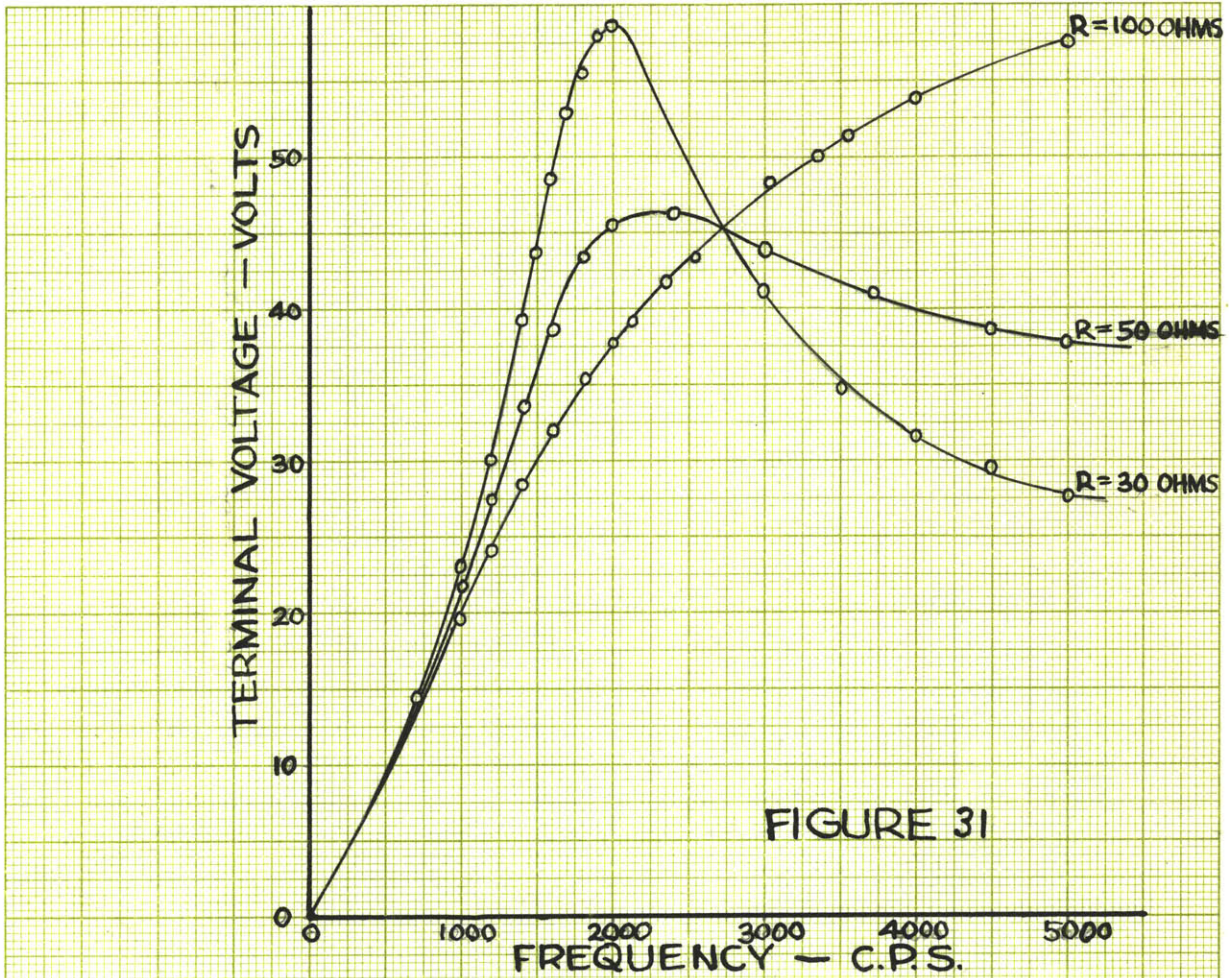


FIGURE 31

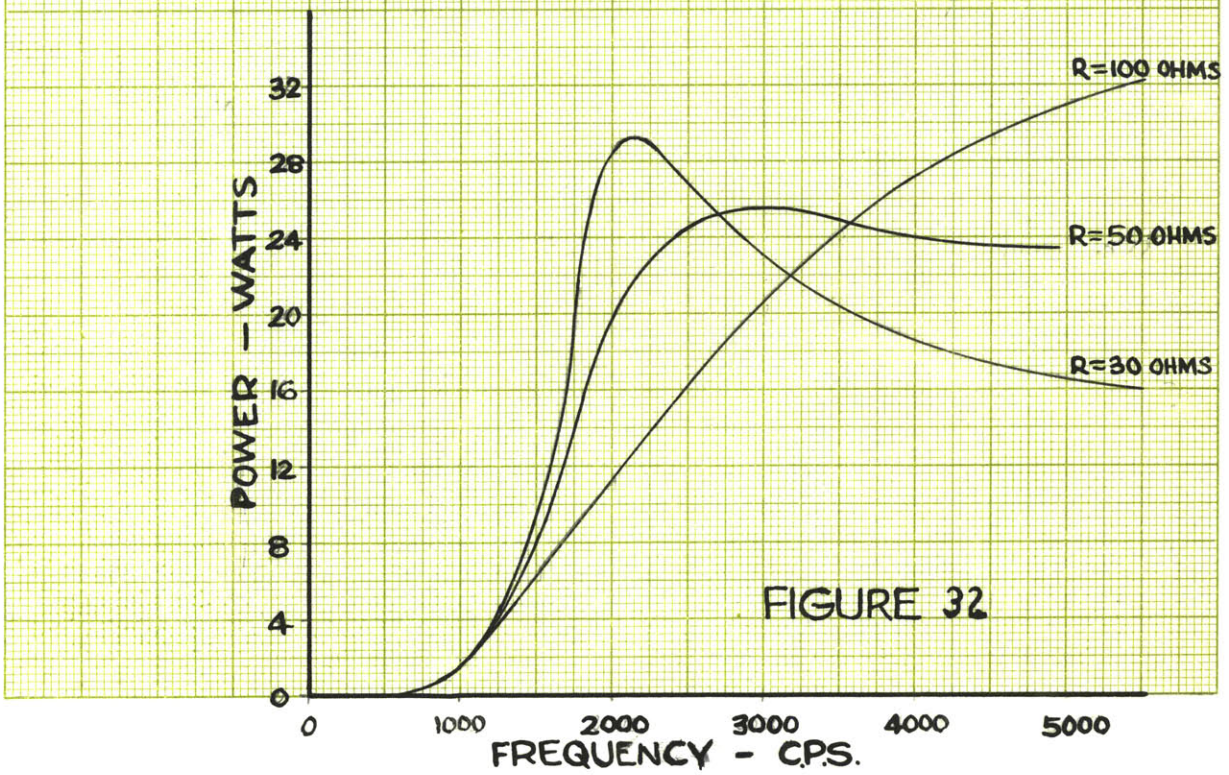


FIGURE 32



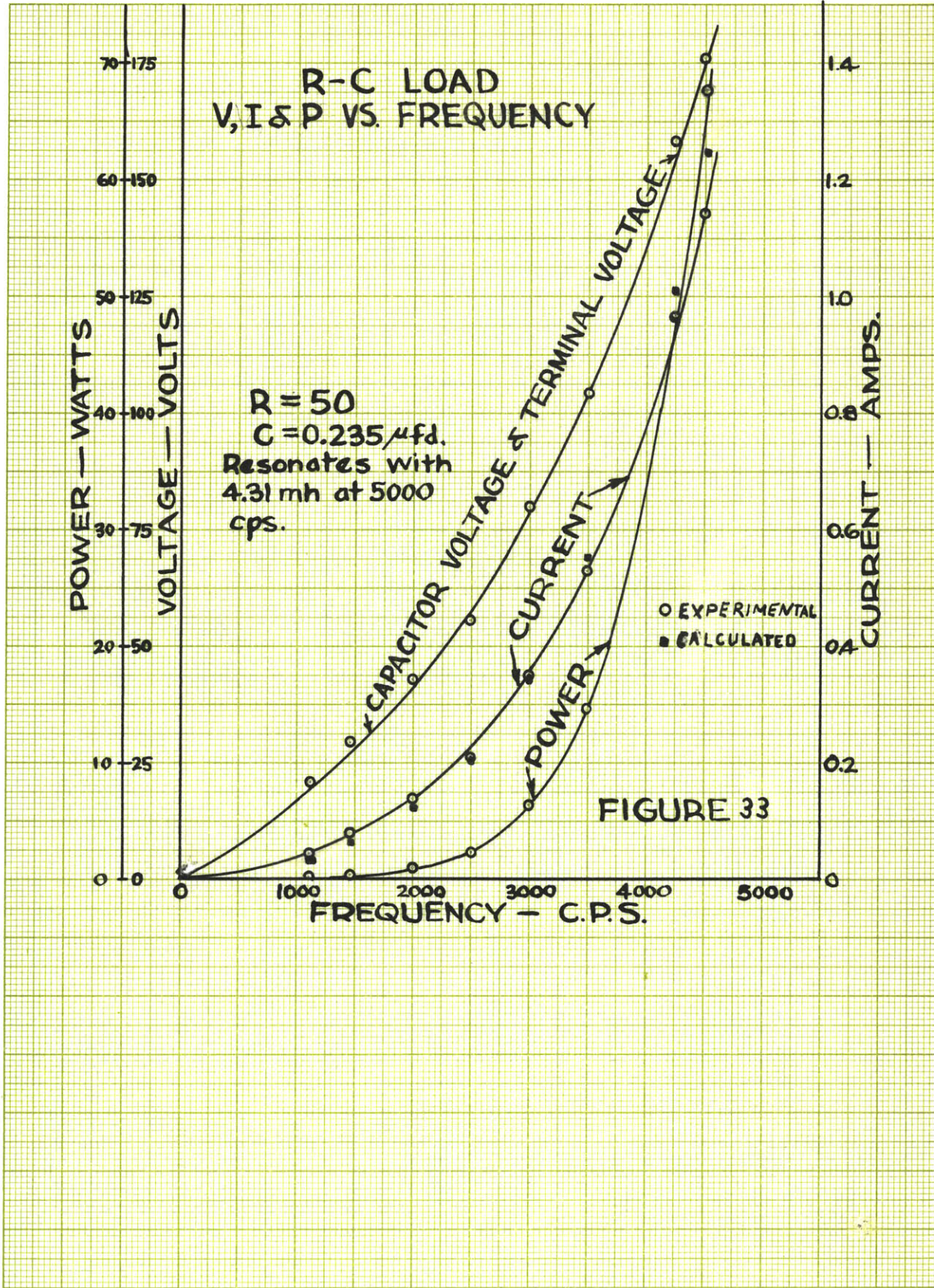
a R - C load. The value of C is adjusted to resonate with the machine inductance at  $f_1$ , and R is made as small as is possible without drawing excessive current. The effective resistance at  $f_1$  is then given by  $R_{\text{eff}} = \frac{Kf_1}{I_1} - R_1$  (the value of  $R_1$  should be carefully measured). This procedure is repeated for other frequencies. \*) Referring again to Figure 29 one finds that the current may or may not have a relative maximum, depending on the value of R. In Appendix III, eq. 2 gives the frequency at which maximum current occurs, if there is one, otherwise the formula indicates that there is no maximum. From this formula the frequency at which maximum current occurs for the three cases is  $f = 2090$  for  $R = 30$ ,  $f = 2840$  for  $R = 50$ , and no maximum for  $R = 100$ . This agrees well with the experimental results.

The capacitor voltage (Fig.30) is a maximum for the resonant frequency. The value of this maximum voltage can be determined from equation 1 in the Appendix III. Thus, for  $R = 30$ ,  $V_{c_{\text{max}}} = 56$ ,  $R = 50$ ,  $V_{c_{\text{max}}} = 36$ , and  $R = 100$ ,  $V_{c_{\text{max}}} = 18.6$ . These values compare favorably with the test points.

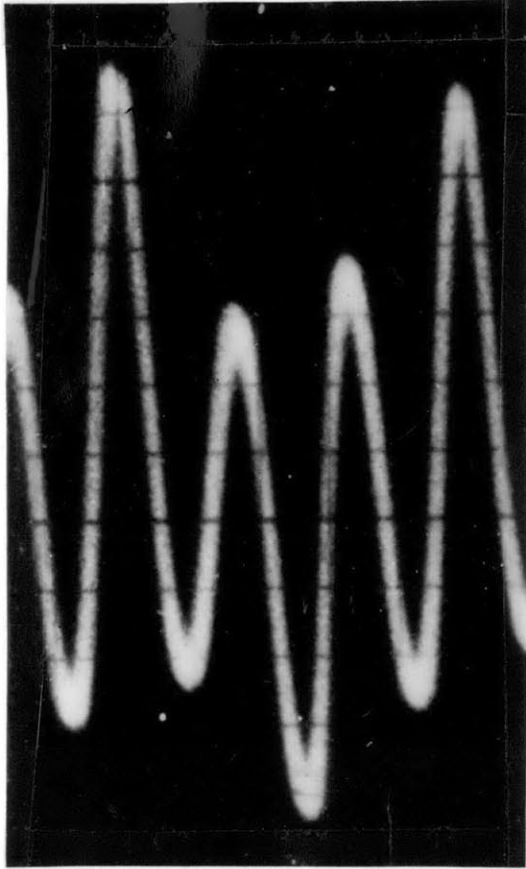
Figure 33 shows again characteristics for a capacitive load where the value of capacitance was selected for resonance at 5000 cps. Note the sharp increase of all variables as the resonant frequency is approached.

---

\*) No data were obtained according to this procedure since the machine became defective before it was realized that this methods may possibly be used to determine  $R_{\text{eff}}$ .

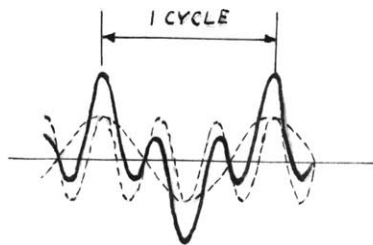


It was stated on page 36 that the fundamental component of the current acting on the double-frequency term of the armature reaction permeance, gives rise to a fundamental and a third harmonic component of flux. This third harmonic flux induces a third harmonic emf. The magnitude of the third harmonic current caused by this emf depends on the impedance offered to currents of this frequency. Figure 34a is a reproduction of the current wave form as it appeared on the oscilloscope when the alternator was driven at 6200 rpm (corresponding to a fundamental frequency of 620 cps), operating into a capacitive load with  $R = 5$  ohms and  $C = 1.47 \mu\text{fd}$ . This value of capacitance resonates with the internal inductance of the alternator at 2000 cps. It then follows that for third harmonic quantities the capacitive reactance nearly neutralizes the internal inductive reactance. Consequently, a large third harmonic current component is set up. Figure 34b will prove helpful in interpreting the wave form of Figure 34a as the result of mainly a fundamental and a third harmonic.



(a)

FIGURE 34



(b)

## V. CONCLUSIONS

The small discrepancy between calculated and experimental results in the preceding chapter indicates that the equivalent circuit of Figure 24 closely simulates the behavior of the alternator over a wide operating range. The equivalent circuit constants,  $K$  and  $L_0$ , were determined from test data since the state of the permanent magnets was not known. In equation 31 these constants were determined for one winding purely from design data assuming that the magnets had been charged to their saturation value. Comparing the two sets of values (where  $L_0$  in equation 31 must be used since the two windings are in parallel) one finds that  $K$  determined from equation 31 is larger than the test value and  $L_0$  from equation 31 is smaller. Under the assumption that the values determined from design data are correct, the discrepancy is explained by the fact that the two sets of values correspond to different states of the permanent magnets. The following question then naturally arises: For rotor and stator given, what excitation should be supplied to obtain maximum output? For maximum output  $K$  should obviously be as large as possible and it is desirable to make  $L_0$  small.  $L_0$  will be small if the iron in the path of the armature reaction flux is saturated. The requirement on  $L_0$ , however, is not very stringent since the effect of  $L_0$  can be neutralized by a series-connected capacitor, if operation is confined to a narrow frequency band. The availability of suitable capacitor in small physical sizes is an outstanding advantage in the application of high-frequency

alternators. For the alternator under investigation a suitable mica or ceramic capacitor would not exceed the size of a 10-cent coin.

We can now concentrate the discussion on K. To simplify matters, assume that the rotor core is not saturated, then Figure 13 applies. (This assumption is not unreasonable since it will usually be possible to make the rotor core deep enough to accommodate the tooth flux). In Figure 13 the operating point lies in a strongly saturated region. The useful maximum alternating flux is given by the distance between lines 4 and 5 and 5 and 1 and is a direct measure of K. Observe that the ratio of permanent magnet flux  $\phi_g$  to useful flux  $\phi_{a_{oc}}$  is large (appr.4). Suppose now that due to a decrease in excitation (diminishing the permanent magnet dimension), the operating point moves toward the left along line 5. This will cause K to increase until the operating point has moved to the ordinate for which the tangent to line 4 is parallel to line 1. Here K reaches a maximum value. It is believed that operation at or near this point will yield maximum output. Note that the ratio of permanent magnet flux to useful flux has been appreciably reduced. There remains to solve the design problem which is twofold (1) to find a magnet which will place the operating point in the region for which K is maximum, (2) to minimize the volume of this magnet. The solution of this problem is found in the paper by Hornfleck and Edgar.\*)

---

\*) Loc. cit.

APPENDIX I

Evaluation of  $P_{\alpha}''$  and  $P_{\beta}''$  for rotor position  $\theta = 0$

---

Figure 1 defines the sections into which the air space must be divided in order to calculate the permeance according to the Substitute-Angle Method. Dimensions are obtained from the drawings included at the end of this appendix. These drawings were supplied by D & R, Ltd. The substitute angle  $\alpha$  is taken as 0.47 radian = 27 degrees, and calculations are performed for a machine of 1 cm axial length. If Figure 1 is considered to be rectified in the sense of the descriptive geometry the following relations apply:

$$P_1 = \frac{.113}{.0025} = 45.2 \text{ cgs units}$$

$$2P_2 = 2 \int_0^{.01} \frac{dr}{.0025 + \beta_1 r}$$

$$\beta_1 = 90 - \alpha - 15^\circ = 48^\circ = .838 \text{ radian}$$

$$2P_2 = \frac{2}{.838} \ln \left( 1 + .838 \frac{.01}{.0025} \right) = 3.5 \text{ cgs units}$$

$$2P_3 = 2 \int_0^{.066} \frac{dr}{.0025 + \beta_1(r + .01) + \beta_2 r}$$

$$\beta_2 = 90 - \alpha - 30 = 33^\circ = .576 \text{ radian}$$

$$2P_3 = 2 \int_0^{.066} \frac{dr}{.0025 + \beta_1 \times .01 + (\beta_1 + \beta_2)r}$$

$$= \frac{2}{1.414} \ln \left( 1 + 1.414 \frac{.066}{.011} \right) =$$

$$\frac{3.2 \text{ cgs units}}{P_{\alpha}'' \approx 52 \text{ cgs units}}$$

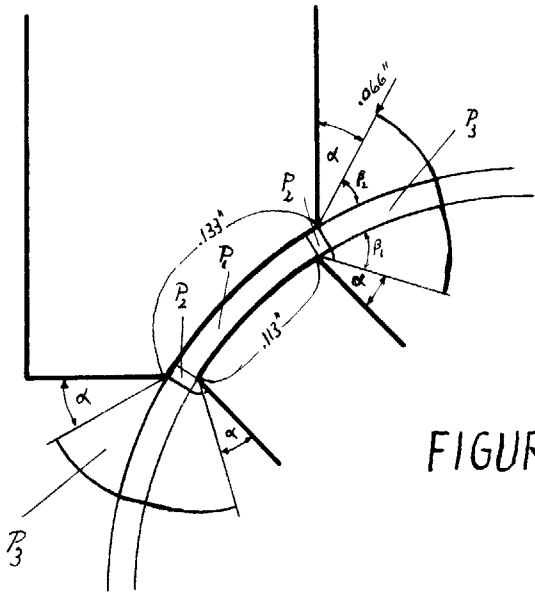


FIGURE 1

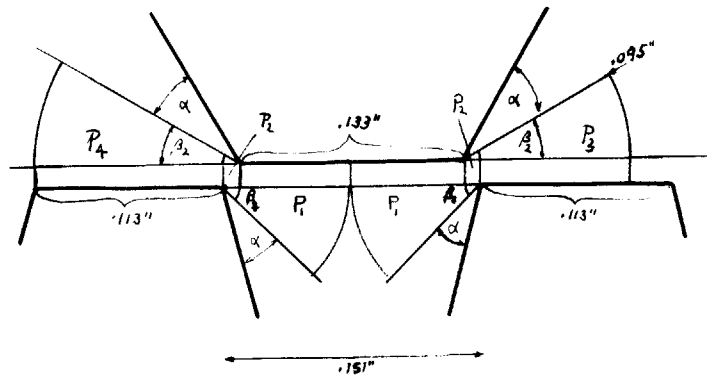


FIGURE 2



Figure 2 pertains to  $P_{\beta}''$  and is shown in developed form.

$$2P_1 = 2 \int_{\frac{.151-.133}{2}}^{.151/2} \frac{dr}{.0025 + \beta_1 r} = \frac{2}{.838} \ln \frac{1 + .838 \frac{.0755}{.0025}}{1 + .838 \frac{.009}{.0025}} = 4.9 \text{ cgs units}$$

$$2P_2 = 2 \int_0^{.009} \frac{dr}{.0025 + \beta_2 r + \beta_1 (.009 - r)} = \frac{2}{\beta_2 - \beta_1} \ln \left( 1 + \beta_2 - \beta_1 \frac{.009}{.01} \right) = 1.6 \text{ cgs units}$$

$$P_3 = \int_{.009}^{.095} \frac{dr}{.0025 + \beta_2 r} = \frac{1}{.576} \ln \frac{1 + .576 \frac{.095}{.0025}}{1 + .576 \frac{.009}{.0025}} = 3.3 \text{ cgs units}$$

$$P_4 = \int_{.009}^{.124} \frac{dr}{.0025 + \beta_2 r} = \frac{1}{.576} \ln \frac{1 + .576 \frac{.124}{.0025}}{1 + .576 \frac{.009}{.0025}} = 3.7 \text{ cgs units}$$

---


$$P_{\beta}'' = 13.5 \text{ cgs units}$$

If similar calculations are performed for  $\theta = 45^\circ$  and

$\theta = 90^\circ$ , one obtains

$$P_{\alpha}'' = 44.5 \quad P_{\beta}'' = 21 \quad \text{for } \theta = 45^\circ$$

$$P_{\alpha}'' = P_{\beta}'' = 34 \quad \text{for } \theta = 90^\circ$$

### Open-Circuit Leakage Permeance

The equivalent diameter of the magnet

$$d = 2 \sqrt{\frac{\text{Area}(\text{total})}{\pi}} = 2 \sqrt{\frac{2.2 \cdot 0.812}{\pi}} = 1.5 \text{ cm,}$$

the length (total) of the magnet

$$l = .87 \times 2.54 = 2.2 \text{ cm}$$

Then the dimensionless ratio

$$l/d = \frac{2.2}{1.5} = 1.47$$

for this ratio of  $l/d$  (from curve) \*)

$$\frac{\text{magnet length}}{\text{magnet area}} P_e = 4.3$$

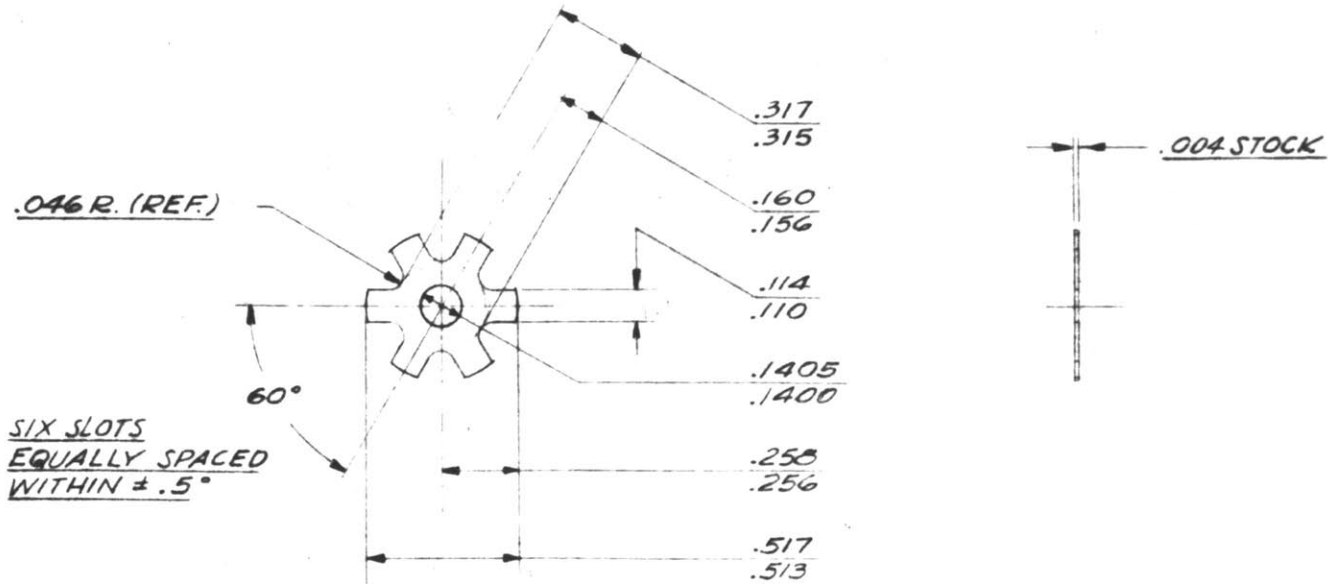
then

$$P_e = 4.3 \frac{1.79}{2.2} = 3.5$$

$$P_e \text{ p.u. axial length} = \frac{3.5}{2.2} = 1.6 \text{ cgs units}$$

---

\*) A.J. Hornfeck and R.F. Edgar, The Output and Optimum Design of Permanent Magnets Subjected to Demagnetizing forces, Trans. AIEE, vol. 59, pp 1017 - 1024, 1940.



215	A14-1200	.004 TRANSFORMER STEEL	ALLEGHENY LUDLUM TYPE A		OXIDIZE
REQ	NEXT ASSEMBLY	MATERIAL	SPEC.	H. T.	FINISH

LIST OF MATERIALS

DRAWN *C E MACDONALD*

CHECKED .....

APPROVED .....

TOLERANCE:

LAMINATION-  
ROTOR

**d & r**  
LTD.

402 E. Gutierrez St.  
SANTA BARBARA, CALIF.

2. TO OXIDIZE: HEAT IN  
OVEN OR OPEN FLAME

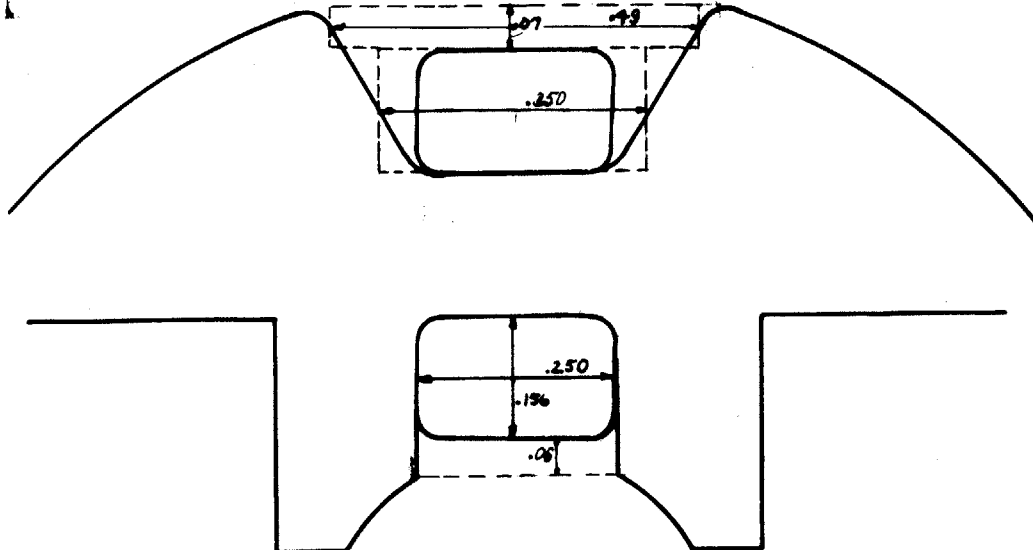
1. REMOVE ROUGH EDGES  
NOTE:

SCALE: TWO TIMES SIZE

**T14-1203**

APPENDIX II

Calculation of Armature Reaction Leakage Permeance  $P_a$



From the accompanying figure

$$P_a = \frac{1}{3} \frac{.156}{.250} + \frac{1}{3} \frac{.156}{.350} + \frac{.06}{.250} + \frac{.07}{.49}$$

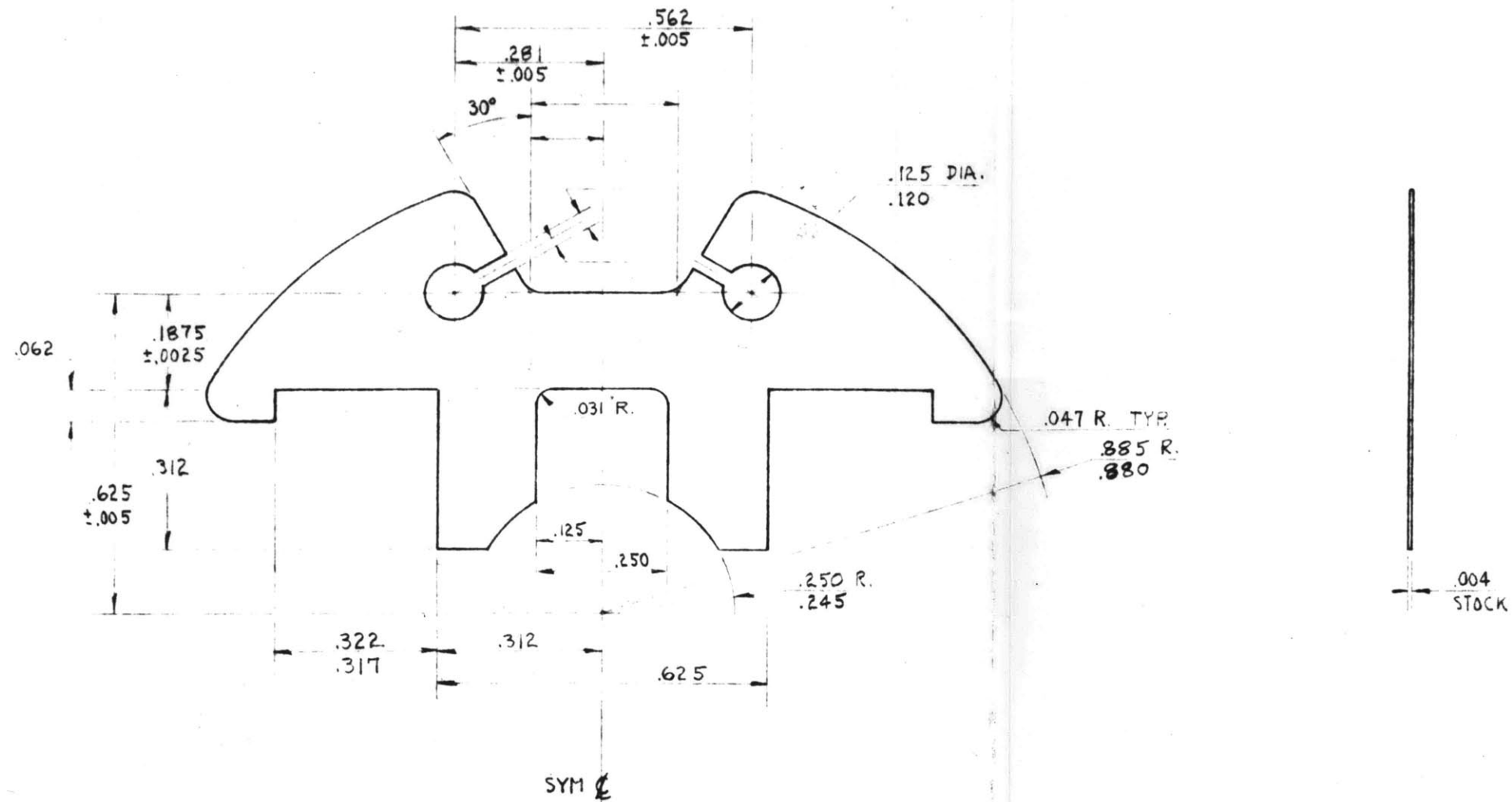
$$= .208 + .164 + .24 + .143 = .755$$

add .145 for flux paths not considered

$$\underline{\underline{P_a = .9 \text{ cgs units}}}$$

---

\*) The factor of 1/3 for the winding areas results from integrating the flux linkages.

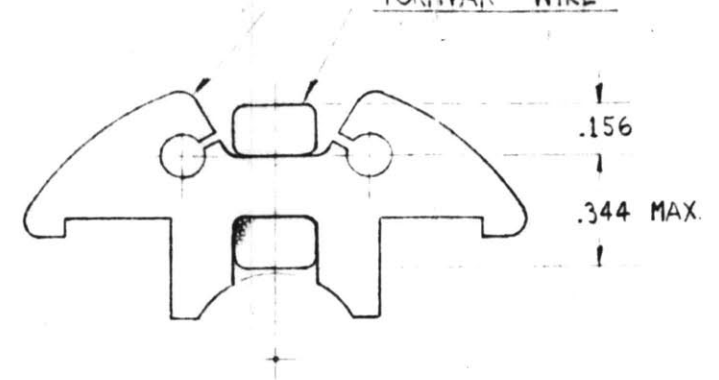
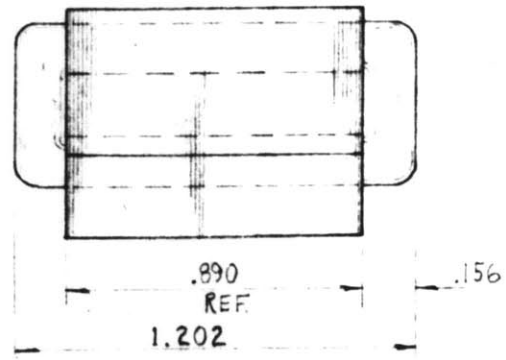



- NOTES:
1. REMOVE ALL BURRS
  2. TO OXIDIZE: HEAT IN OVEN OR OPEN FLAME

REQ	T14-1102	.004 TRANSFORMER STEEL	ALLEGHENY LUDLUM TYPE A	H. T.	OXIDIZE
	NEXT ASSEMBLY	MATERIAL	SPEC.		FINISH
LIST OF MATERIALS					
DRAWN	SWANSON	7-15-52	LAMINATION- STATOR		<b>d &amp; r</b> LTD. 402 E. Gallows St. SANTA BARBARA, CALIF.
CHECKED					
APPROVED					
TOLERANCE:			SCALE: 4X SIZE		T14-1101
DECIMAL: ±.003					
ANGULAR: ± 1°					

T14-1102  
 LAM. ASSEM.-1 REQ

180 TURNS #31 HEAVY  
 FORMVAR WIRE



1	T14-1100				
REQ	NEXT ASSEMBLY	MATERIAL	SPEC.	H. T.	FINISH
LIST OF MATERIALS					
DRAWN SWANSON 7-17-52		STATOR + COIL ASSEM		 402 E. Gallenas St. SANTA BARBARA, CALIF.	
CHECKED _____					
APPROVED _____					
TOLERANCE:		SCALE: 2X SIZE		T14-1103	
DECIMAL: ± .020					

APPENDIX III

Data for Figure 25, no-load voltage vs. frequency

f	V <sub>oc</sub>	f	V <sub>oc</sub>	
630	11.2	2800	50	from which
1460	26	3400	60.5	K = 0.0178 Volt/cps
2000	36	4000	70.5	
		5000	89	

The short-circuit current according to the test described on p.41 was found to be

$$I_{sc} = 0.655 \text{ amp.}, \text{ then from eq.33}$$

$$L_0 = \frac{K}{2\pi I_{sc}} = \frac{0.0178}{2\pi \cdot 0.655} = 4.32 \text{ mh}$$

Data and calculations for Figure 27 (Resistive Load)

f = 2000 cps

measured			P = V <sub>T</sub> I	calculated		
R	I	V <sub>T</sub>		I	V <sub>T</sub>	P
	0	35.6	0			
251	.135	34	4.6	.137	34.4	4.72
201	.163	33.2	5.41			
151	.214	32.3	6.92	.218	33	7.19
101	.295	29.8	8.80	.303	30.7	9.3
81	.34	27.9	9.50			
71	.372	26.7	9.95			
61	.405	25.0	10.1			
51	.444	23.0	10.2	.465	23.7	10.9
41	.485	20.3	9.85			
36	.51	18.7	9.53			
31	.535	16.9	9.05			
26	.56	15.0	8.36	.581	15.2	8.75
16	.60	10.1	5.82	.624	10.1	6.25
0	.655	0	0			

Sample Calculation

R = 251 with f = 2000 cps.  
 E = K<sub>f</sub> = 35.6; ωL<sub>0</sub> = 54.2 ohms  
 Z = 251 + R<sub>eff</sub> + j 54.2  
 R<sub>eff</sub> = 2.6

(Z) = 260  
 I =  $\frac{35.6}{260} = 0.137$   
 V = IR = 0.137 \* 251 = 34.4  
 P = VI = 34.4 \* 0.137 = 4.72

b)  $f = 3000$  cps.

measured				calculated		
R	I	$V_T$	$P=V_T I$	I	$V_T$	P
402	.128	51.8	6.64	.129	52.0	6.66
304	.165	50.5	8.33			
202	.235	47.6	11.2	.241	48.7	11.7
152	.295	45	13.4			
132	.326	43.5	14.2			
102	.384	39.5	15.2	.398	40.6	16.15
77	.447	35.0	15.65	.468	36	16.95
68	.475	32.4	15.4	.494	33.6	16.5
52	.52	27.3	14.2			
42	.55	23.4	12.9	.575	24.2	13.9
27	.60	16.8	9.7			

Data and calculations for Figures 29, 30, 31, 32 (R-C Load)

a)  $C = 1.47 \mu\text{fd}$   $R = 31$  ohms

Sample Calculation

$$f = 1000 \text{ cps}, \omega L_0 = 2\pi 1000 \cdot 4.32 \times 10^{-3} = 27.1 \Omega, \frac{1}{\omega C} = \frac{10^6}{2\pi 1000 \cdot 1.47} = 108.2$$

$$Z = \sqrt{(31 + 2.6)^2 + (108.2 - 27.1)^2} = 88$$

$$E = Kf = 0.0178 \cdot 1000 = 17.8 ; I = \frac{E}{Z} = \frac{17.8}{88} = 0.202$$

Data on next page.



C = 1.47 fd R = 31 ohms

f	measured			P=I <sub>T</sub> <sup>2</sup> R	calculated							
	I <sub>T</sub>	V <sub>C</sub>	V <sub>T</sub>		ωL <sub>O</sub>	$\frac{1}{\omega C}$	$ \omega L_O - \frac{1}{\omega C} $	I <sub>T</sub>	X <sub>C</sub>	Z	Kf	I
710	.104	14	14.3	--	19.3	152.5	133.2	15.85			17.8	
1000	.210	21.8	23	--	27.1	108.2	81.1	22.8	88		↓	.202
1200	.318	28.2	30	3.13	32.7	90.4	57.7	28.8	--	--	--	--
1400	.48	36.5	39.1	--	38	77.4	39.4	37.1	--	--	--	--
1500	.57	40.5	43.6	9.75	40.7	72.2	31.5	41.2	46	26.8	.582	
1600	.665	44.2	48.5	--	43.4	67.7	24.3	44.7	--	--	--	--
1700	.765	47.8	52.7	18.1	46.1	63.7	17.6	48.6	--	--	--	--
1800	.84	50	55.5	--	48.8	60.3	11.5	50.7	--	--	--	--
1900	.92	51.5	58	26.2	51.5	57	5.5	52.4	--	--	--	--
2000	.968	51.5	58.7	28.5	54.2	54.2	0	52.4	33.6	35.6	1.06	
5000	.74	16	27.5	16.5	135.5	21.6	113.9	16	119	89	.748	
4500	.76	18.2	29.5	--	122	24.1	98	18.2	103.8	80.2	.774	
4000	.785	21.3	31.5	19.1	108.2	27.1	81.1	21.3	88	71.2	.81	
3500	.81	25	34.5	--	94.7	31	63.7	25.1	72.1	62.4	.865	
3000	.88	31.5	41	23	81.3	36.1	45.2	31.7	56.3	53.4	.948	
2500	--	--	--	--	67.8	43.3	24.5	--	41.9	44.5	1.06	

C = 1.47  $\mu$ fd R = 51.4 ohms

f	measured			P=I <sub>T</sub> <sup>2</sup> R	calculated							
	I <sub>T</sub>	V <sub>c</sub>	V <sub>T</sub>		$\omega L_0$	$\frac{1}{\omega C}$	$ \omega L_0 - \frac{1}{\omega C} $	I <sub>T</sub>	X <sub>C</sub>	Z	Kf	I
765	.104	13.9	15.3	--	20.7	141.5	119.8	14.7	--	--	--	
1010	.184	19.4	21.6	--	27.4	107	79.6	19.7	96.4	18	.187	
1200	.268	23.6	27.4	--	32.5	90.4	57.9	24.2	--	--	--	
1416	.372	28.2	33.5	7.05	38.4	76.5	38.1	28.4	--	--	--	
1600	.458	31	38.5	--	43.4	67.6	24.2	31	--	--	--	
1800	.56	33	43.3	--	48.8	60.4	11.6	33.8	55.1	32	.581	
2000	.62	33.1	45.5	19.6	54.2	54.2	0	33.6	54	35.6	.66	
2350	.67	32	46.1	--	63.7	46.0	17.6	30.9	--	--	--	
5000	.692	14.6	37.6	23.8	137	21.7	115.3	15	128	89	.695	
4500	.691	16.6	38.6	--	122	24.1	97.9	16.6	112	80.1	.715	
3700	.7	20.7	41	24.5	100	29.3	70.7	20.7	89	65.9	.79	
3000	.705	25.7	44	24.6	81.3	36.1	45.2	25.5	70.5	53.4	.757	

C = 1.47  $\mu$ fd R = 102 ohms

f	measured			P=I <sub>T</sub> <sup>2</sup> R	$\omega L_0$	calculated					
	I <sub>t</sub>	V <sub>C</sub>	V <sub>T</sub>			$\frac{1}{\omega C}$	$ L_0 - \frac{1}{\omega C} $	I <sub>t</sub> X <sub>C</sub>	Z	Kf	I
658	.064	10.2	12.4	--	17.8	164.5	146.7	10.5	--	---	---
815	.0948	12.1	15.8	--	22.1	133	110.9	12.6	--	---	---
1000	.135	14	19.6	1.86	27.1	108.2	81.1	14.6	133	17.8	.134
1200	.178	15.5	24	--	32.7	90.4	57.7	16.1	--	---	---
1410	.225	16.6	28.4	--	38.2	76.9	38.7	17.3	--	---	---
1620	.266	17.1	32	--	43.9	67	23.1	17.8	--	---	---
1820	.303	17.4	35.3	--	49.3	59.6	10.3	18	--	---	---
2000	.33	17.4	37.7	11.1	54.2	54.2	0	17.9	104.4	35.6	.34
2125	.349	17.38	39	--	57.6	51	6.6	17.8	--	---	---
2350	.375	17.2	41.8	--	63.6	46.2	17.4	17.3	--	---	---
2550	.40	16.9	43.8	16.3	69	42.5	26.5	17	108	45.4	.42
3025	.451	15.8	48.3	20.8	82	35.8	44.2	16.1	113.6	53.8	.472
3350	.471	15.2	50.1	--	90.8	32.4	58.4	15.2	--	---	---
3550	.487	14.6	51.5	--	96.2	30.5	65.7	14.8	--	---	---
4000	.52	13.6	53.8	27.5	108.2	27.1	81.1	14.1	133	71.1	.535
5000	.552	11.7	57.5	31	135.5	21.6	113.9	11.9	155	89	.574

From the equivalent circuit, the voltage across the capacitor

$$V_c = \frac{Kf}{\sqrt{(R_{\text{eff}} + R)^2 + (\omega L_0 - \frac{1}{\omega C})^2}} \frac{1}{\omega C}$$

$$= \frac{K}{2\pi C \sqrt{(R_{\text{eff}} + R)^2 + (\omega L_0 - \frac{1}{\omega C})^2}}$$

and is obviously a maximum at the resonant frequency

$$f_r = \frac{1}{2\pi \sqrt{L_0 C}}$$

then

$$V_{c/\text{max}} = \frac{K}{2\pi(R_{\text{eff}} + R)C} \quad (1)$$

Similarly the current

$$I = \frac{Kf}{\sqrt{(R_{\text{eff}} + R)^2 + (\omega L_0 - \frac{1}{\omega C})^2}} = \frac{K}{\sqrt{\left[\frac{R_{\text{eff}} + R}{f}\right]^2 + \left[2\pi L_0 - \frac{1}{2\pi f^2 C}\right]^2}}$$

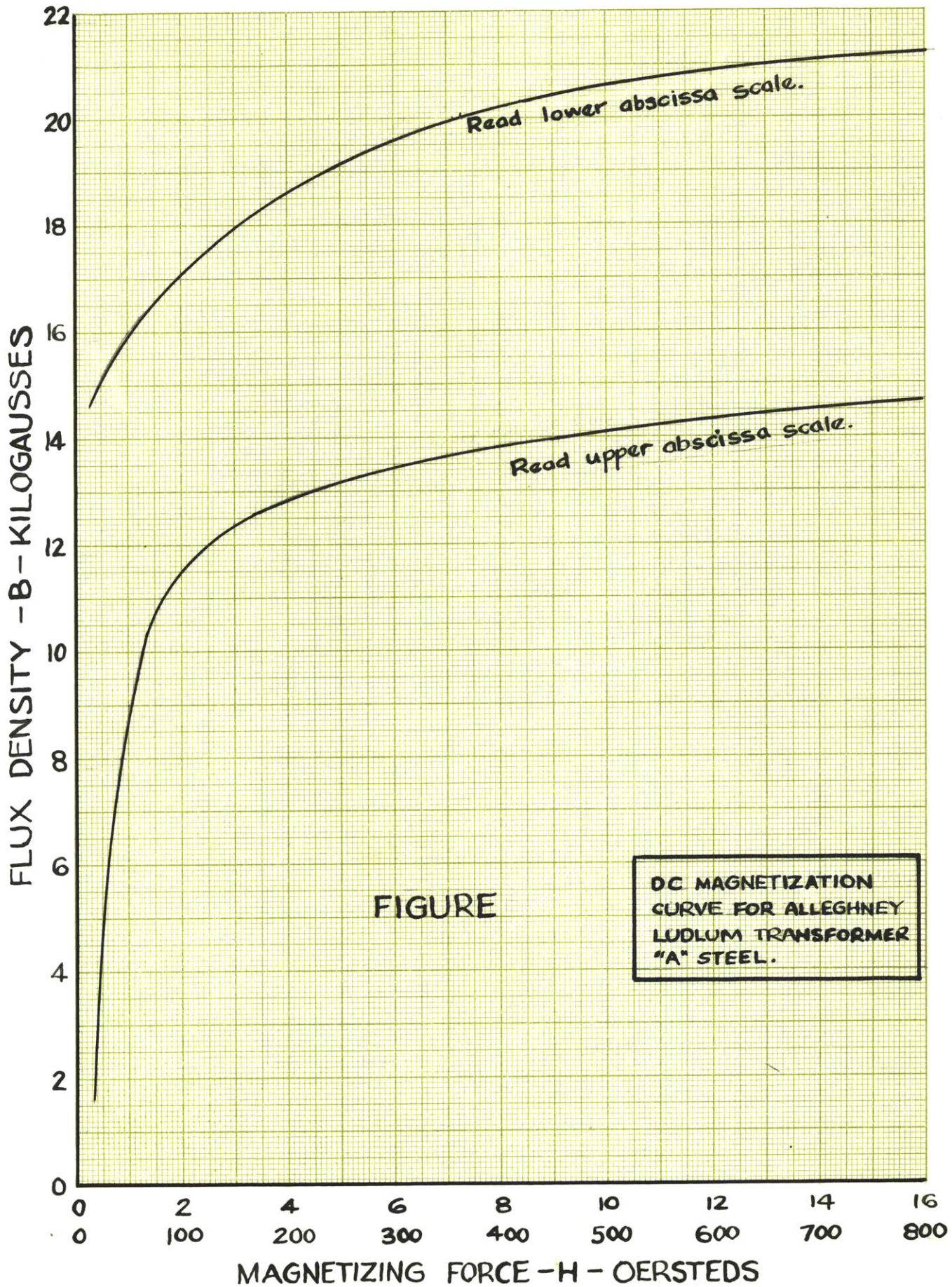
To find the frequency for which the current is a maximum, one forms

$$\frac{d}{df} \left[ \left( \frac{R_{\text{eff}} + R}{f} \right)^2 + \left( 2\pi L_0 - \frac{1}{2\pi f^2 C} \right)^2 \right]$$

$$= -2 \frac{(R_{\text{eff}} + R)^2}{f^3} + 2 \left( 2\pi L_0 - \frac{1}{2\pi f^2 C} \right) \frac{1}{\pi f^3 C} = 0$$

after some rearranging, the frequency at which the current is a maximum is obtained as

$$f_{I_{\text{max}}} = \frac{f_r}{\sqrt{1 - \frac{(R_{\text{eff}} + R)^2}{L_0/C}}} \quad \text{with } f_r = \frac{1}{2\pi \sqrt{L_0 C}} \quad (2)$$



## BIBLIOGRAPHY

1. Hornfleck and Edgar, "The Output and Optimum Design of Permanent Magnets Subjected to Demagnetizing Forces," AIEE Transactions, Vol. 59, Pages 1017-1024, 1940.
2. The India Steel Product Company, Permanent Magnet Manual No 4
3. Robert Pohl, "Theory of Pulsating-Field Machines," JIEE (London), Vol. 93, Part II, Page 37, 1946.
4. R. Richter, "Kurzes Lehrbuch der Elektr. Maschinen," Pages 92-103, Springer-Verlag, 1949.
5. H.C. Roters, "Electromagnetic Devices," Chapter V, John Wiley & Sons, Inc., New York.
6. R.L. Sanford, "Permanent Magnets," Circular of the National Bureau of Standards, C 448, 1944.
7. K.L. Scott, "Magnet Steels and Permanent Magnets," AIEE Transactions, Vol. 51, Pages 410-417, 1932.
8. J.H. Walker, "High Frequency Alternators," JIEE (London), Vol. 93, Part II, Pages 67-80